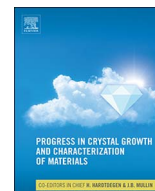




Contents lists available at ScienceDirect

# Progress in Crystal Growth and Characterization of Materials

journal homepage: [www.elsevier.com/locate/pcrysgrow](http://www.elsevier.com/locate/pcrysgrow)

Full length Article

## Molecular beam epitaxy as a growth technique for achieving free-standing zinc-blende GaN and wurtzite $\text{Al}_x\text{Ga}_{1-x}\text{N}$

S.V. Novikov\*, A.J. Kent, C.T. Foxon

School of Physics and Astronomy, University of Nottingham, Nottingham, NG7 2RD, UK

### A B S T R A C T

Currently there is a high level of interest in the development of ultraviolet (UV) light sources for solid-state lighting, optical sensors, surface decontamination and water purification. III-V semiconductor UV LEDs are now successfully manufactured using the AlGaIn material system; however, their efficiency is still low. The majority of UV LEDs require  $\text{Al}_x\text{Ga}_{1-x}\text{N}$  layers with compositions in the mid-range between AlN and GaN. Because there is a significant difference in the lattice parameters of GaN and AlN,  $\text{Al}_x\text{Ga}_{1-x}\text{N}$  substrates would be preferable to those of either GaN or AlN for many ultraviolet device applications. However, the growth of  $\text{Al}_x\text{Ga}_{1-x}\text{N}$  bulk crystals by any standard bulk growth techniques has not been developed so far.

There are very strong electric polarization fields inside the wurtzite (hexagonal) group III-nitride structures. The charge separation within quantum wells leads to a significant reduction in the efficiency of optoelectronic device structures. Therefore, the growth of non-polar and semi-polar group III-nitride structures has been the subject of considerable interest recently. A direct way to eliminate polarization effects is to use non-polar (001) zinc-blende (cubic) III-nitride layers. However, attempts to grow zinc-blende GaN bulk crystals by any standard bulk growth techniques were not successful.

Molecular beam epitaxy (MBE) is normally regarded as an epitaxial technique for the growth of very thin layers with monolayer control of their thickness. In this study we have used plasma-assisted molecular beam epitaxy (PA-MBE) and have produced for the first time free-standing layers of zinc-blende GaN up to 100  $\mu\text{m}$  in thickness and up to 3-inch in diameter. We have shown that our newly developed PA-MBE process for the growth of zinc-blende GaN layers can also be used to achieve free-standing wurtzite  $\text{Al}_x\text{Ga}_{1-x}\text{N}$  wafers. Zinc-blende and wurtzite  $\text{Al}_x\text{Ga}_{1-x}\text{N}$  polytypes can be grown on different orientations of GaAs substrates - (001) and (111)B respectively. We have subsequently removed the GaAs using a chemical etch in order to produce free-standing GaN and  $\text{Al}_x\text{Ga}_{1-x}\text{N}$  wafers. At a thickness of  $\sim 30 \mu\text{m}$ , free-standing GaN and  $\text{Al}_x\text{Ga}_{1-x}\text{N}$  wafers can easily be handled without cracking. Therefore, free-standing GaN and  $\text{Al}_x\text{Ga}_{1-x}\text{N}$  wafers with thicknesses in the 30–100  $\mu\text{m}$  range may be used as substrates for further growth of GaN and  $\text{Al}_x\text{Ga}_{1-x}\text{N}$ -based structures and devices.

We have compared different RF nitrogen plasma sources for the growth of thick nitride  $\text{Al}_x\text{Ga}_{1-x}\text{N}$  films including a standard HD25 source from Oxford Applied Research and a novel high efficiency source from Riber. We have investigated a wide range of the growth rates from 0.2 to 3  $\mu\text{m}/\text{h}$ . The use of highly efficient nitrogen RF plasma sources makes PA-MBE a potentially viable commercial process, since free-standing films can be achieved in a single day.

Our results have demonstrated that MBE may be competitive with the other group III-nitrides bulk growth techniques in several important areas including production of free-standing zinc-blende (cubic) (Al)GaN and of free-standing wurtzite (hexagonal) AlGaIn.

### 1. Introduction

There is currently a high level of interest both commercial and scientific in nitride semiconductors for light emitting, high-power, high-frequency and high temperature electronic devices. Group III-nitride layers for device fabrication are normally grown by three main

methods; metal-organic vapour phase epitaxy (MOVPE), hydride vapour phase epitaxy (HVPE) and molecular beam epitaxy (MBE). The biggest problem for nitrides is the lack of suitable lattice-matched substrates. Therefore, AlGaIn layers are grown on non-lattice matched sapphire, GaAs or SiC substrates. Bulk substrates, matched in lattice constant and thermal expansion properties to epitaxial nitride layers

\* Corresponding author.

E-mail address: [Sergei.Novikov@Nottingham.ac.uk](mailto:Sergei.Novikov@Nottingham.ac.uk) (S.V. Novikov).<http://dx.doi.org/10.1016/j.pcrysgrow.2017.04.001>0960-8974/ © 2017 The Author(s). Published by Elsevier Ltd. This is an open access article under the CC BY license (<http://creativecommons.org/licenses/by/4.0/>).

are required for fabrication of the highest-quality AlGaInN-based devices.

The group III-nitrides normally crystallise in the wurtzite (hexagonal) structure. The unique feature of wurtzite group III-nitrides, in comparison with conventional III-V semiconductors, is the existence of very strong electric polarization fields inside the crystal structure [1]. The charge separation within quantum wells leads to a significant reduction in the efficiency of optoelectronic device structures, due to the reduced overlap of the electron and hole wavefunctions. The electric fields can be eliminated or reduced in wurtzite material by growing in the non-polar or semi-polar directions. Therefore, the growth of non-polar and semi-polar group III-nitride structures has been the subject of considerable interest [2–4].

A direct way to eliminate polarization effects is to use non-polar (001) zinc-blende (cubic) III-nitride layers. The thermodynamically metastable cubic GaN layers have received less attention than the more familiar hexagonal III-N films. However, successful pioneering epitaxial growth of the metastable zinc-blende polytype of GaN has been achieved by various groups more than 20 years ago [5–14]. Interest in zinc-blende GaN is gradually increasing since then for three main reasons: 1) the absence of spontaneous and piezo-electric polarisation fields in cubic GaN [15]; 2) the ability to cleave cubic GaN on the perpendicular {110} cleavage planes for device fabrication; and 3) the enhanced mobility of the carriers (particularly p-type [16]), due in part to the higher crystal symmetry. It has been also suggested theoretically, that Auger interband losses in the blue-green region of the spectrum could be smaller for cubic InGaIn devices in comparison with the hexagonal ones [17].

However, the current state of the availability of zinc-blende bulk GaN substrates is even worse than with bulk hexagonal GaN substrates. There were no reports on the growth of zinc-blende GaN bulk crystals and substrates, and all attempts to achieve bulk cubic GaN substrates have so far failed. It is well established that it is possible to initiate the growth of GaN, AlN and InN layers in the zinc-blende structure on cubic (001) substrates under special growth conditions by MBE, HVPE and MOVPE. Normally cubic GaAs or SiC substrates are used for the growth of thin ( $< 1 \mu\text{m}$ ) cubic nitride layers. It has been shown that cubic GaN, with the lowest content of the hexagonal phase GaN can be grown by MBE [18]. In HVPE, and especially in MOVPE, due to higher growth temperatures, the hexagonal fraction rapidly increases with increasing GaN layer thickness, even when the films were grown on the top of pure cubic GaN MBE buffer layers [18].

There is a significant difference in the lattice parameters of zinc-blende GaN and AlN, unlike the case of GaAs and AlAs. There are only a limited number of publications on the on the growth of very thin zinc-blende AlN layers [19–25] and there are no reports on the growth of bulk zinc-blende AlN crystals so far.

The recent development of group III nitrides allows researchers world-wide to consider  $\text{Al}_x\text{Ga}_{1-x}\text{N}$  based light emitting diodes (LEDs) as a possible new alternative deep ultra-violet (DUV) light source for surface decontamination and water purification [26–30]. If efficient devices can be developed they will be easy to use, have potentially a long life time, be mechanically robust and will lend themselves to battery operation to allow their use in remote locations. Changing the composition of the active  $\text{Al}_x\text{Ga}_{1-x}\text{N}$  layer, will allow one to tune easily the wavelength of the LEDs. This has stimulated research world-wide to develop  $\text{Al}_x\text{Ga}_{1-x}\text{N}$  based DUV LEDs [27–30]. Such DUV LEDs will also have potential applications for drug detection and power electronics.

The first successful semiconductor UV LEDs are now manufactured using the wurtzite  $\text{Al}_x\text{Ga}_{1-x}\text{N}$  material system, covering the energy range from 3.4 up to 6.2 eV One of the most severe problems hindering the progress of DUV LEDs is the lack of suitable substrates on which lattice-matched  $\text{Al}_x\text{Ga}_{1-x}\text{N}$  films can be grown [26–30]. Currently the majority of wurtzite  $\text{Al}_x\text{Ga}_{1-x}\text{N}$  DUV LED devices are grown on sapphire or AlN. The lattice mismatch between the substrate (sapphire or AlN) and the active  $\text{Al}_x\text{Ga}_{1-x}\text{N}$  layers results in poor structural quality of the

layers, cracks, and low radiative recombination rates in current DUV LED devices. Therefore, the AlGaIn layers contain a high density of dislocations arising from the large lattice mismatch and the difference in thermal expansion coefficient between the wurtzite  $\text{Al}_x\text{Ga}_{1-x}\text{N}$  layers and sapphire. This results in a low  $\sim 1$  to 10% external quantum efficiency (EQE) and poor reliability of existing DUV LEDs. DUV LEDs require  $\text{Al}_x\text{Ga}_{1-x}\text{N}$  layers with an AlN content in the mid-range between pure AlN and GaN, and therefore high quality ternary  $\text{Al}_x\text{Ga}_{1-x}\text{N}$  substrates may significantly improve the properties of the devices. However, so far only limited success has been achieved in the growth of bulk ternary wurtzite  $\text{Al}_x\text{Ga}_{1-x}\text{N}$  crystals with a variable AlN content [31,32]

In this article we review the work on the growth of free-standing GaN and  $\text{Al}_x\text{Ga}_{1-x}\text{N}$  by plasma-assisted molecular beam epitaxy (PA-MBE). We discuss first the growth and properties of free-standing zinc-blende (cubic) GaN. We then discuss the growth and properties of free-standing zinc-blende (cubic) and wurtzite (hexagonal)  $\text{Al}_x\text{Ga}_{1-x}\text{N}$  alloys with controlled concentrations of Al. Finally, we discuss the use of high efficiency nitrogen plasma sources to obtain growth rates of 2–3  $\mu\text{m}/\text{h}$  enabling free-standing GaN and  $\text{Al}_x\text{Ga}_{1-x}\text{N}$  samples to be grown in a single day.

### 1.1. MBE of free-standing zinc-blende GaN

We have demonstrated, for the first time, that it is possible to grow free-standing zinc-blende GaN layers by MBE [33–35]. Undoped thick cubic GaN films were grown on semi-insulating cubic GaAs (001) substrates by plasma-assisted molecular beam epitaxy (PA-MBE). MBE is normally regarded as an epitaxial technique for the growth of very thin layers with monolayer control of their thickness. However, we have used the MBE technique and we have produced free-standing GaN layers up to 100  $\mu\text{m}$  in thickness and up to 3-inch in diameter.

Undoped, thick cubic GaN films were grown by PA-MBE in a custom made MBE system and in a standard MOD-GENII system using arsenic ( $\text{As}^2$ ) as a surfactant to initiate the growth of cubic phase material [33–35]. We have used  $\frac{1}{4}$  of 2-inch, 2-inch and 3-inch diameter (001) semi-insulating and n-doped GaAs wafers. The substrate temperature was measured using an optical pyrometer. Growth temperatures of  $\sim 700 \text{ }^\circ\text{C}$  were used. The active nitrogen for the growth of the group III-nitrides was provided by either a CARS25 or an HD25 RF activated plasma source from Oxford Applied Research. Prior to the growth of the GaN layers, a GaAs buffer layer was grown on the GaAs substrate in order to improve the properties of the cubic GaN layers. Free standing GaN layers were obtained by removing the GaAs substrates using a chemical etch (20 ml  $\text{H}_3\text{PO}_4$ : 100 ml  $\text{H}_2\text{O}_2$ ). Samples were studied in-situ using reflection high-energy electron diffraction (RHEED) and after growth ex-situ measurements were performed using X-ray diffraction (XRD), Hall and photoluminescence (PL).

The first thick cubic GaN layers were grown over several days. The GaN samples were grown for several hours each working day, but growth was stopped during the night. However, we realised later that we could sustain a  $24 \times 7$  MBE growth process and subsequently all the long growths were done without interruption.

Fig. 1 shows the dependence of the thickness of zinc-blende GaN on growth time under fixed MBE growth conditions. The GaN film thickness was measured using optical methods for the thinner ( $< 10 \mu\text{m}$ ) films (before removing them from GaAs) and using a micrometer for the thicker films (after removing them from the GaAs substrate). The GaN thickness increased linearly with the growth time and the growth rate was  $\sim 0.3 \mu\text{m}/\text{h}$ . We did not observe any significant change in the growth rate with increasing GaN layer thickness. Even though this growth rate is not particularly fast, it was already comparable to the growth rates for bulk wurtzite GaN crystals grown from the liquid Ga at high pressure [36].

It was possible to obtain free-standing cubic GaN layers for films grown under both Ga- and N-rich conditions even for layers under one

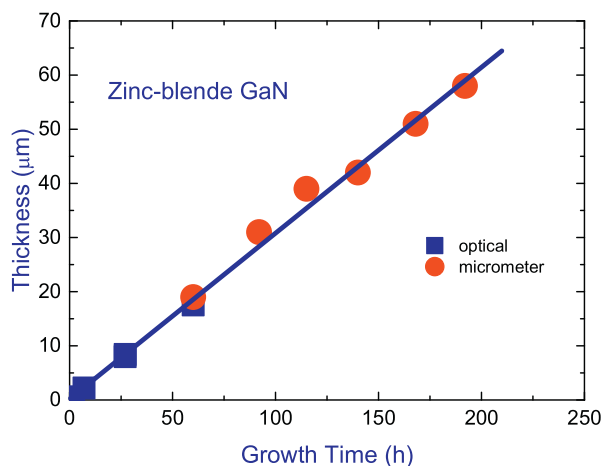


Fig. 1.. The sample thickness versus growth time for zinc-blende GaN grown by PA-MBE.



Fig. 2.. A thin zinc-blende GaN layer mounted on glass after removing the GaAs substrate [35].

micron thick. We have mounted the GaN/GaAs samples on glass using wax and subsequently etched off the GaAs substrate. Unfortunately, due to the strong internal strain, thin ( $< 1 \mu\text{m}$ ) free-standing cubic GaN layers crack and bend into rolls. In Fig. 2 one can see a thin GaN layer on the glass.

With increasing zinc-blende GaN thickness, the samples become stronger and we do not observe any cracks in thicker samples. Fig. 3

shows free-standing zinc-blende GaN layers with a surface area  $> 1 \text{ cm}^2$ . The thickness of the layer shown in Fig. 3(a) is about  $8 \mu\text{m}$ . It can be seen that the free-standing zinc-blende GaN layer is transparent and has the perpendicular  $\{110\}$  cleavage planes associated with cubic symmetry. Also shown in Fig. 3b is a  $30 \mu\text{m}$  sample that can be handled without cracking.

Zinc-blende GaN is the thermodynamically metastable polytype of GaN and under the majority of growth conditions GaN will naturally grow in the form of the wurtzite polytype. For our specific MBE growth conditions we have forced GaN to grow zinc-blende by using (001) cubic GaAs substrates and by supplying an additional  $\text{As}^2$  flux. It is difficult to initiate the growth of zinc-blende GaN, but it is even more difficult to sustain the growth of the pure zinc-blende polytype in thick layers without any wurtzite inclusions. Small wurtzite inclusions are formed inside the zinc-blende GaN probably due to thermodynamic instabilities, however, the precise mechanism for the formation of such inclusions is still unknown. The initial step in the growth of free-standing zinc-blende GaN crystals is crucial for suppression of the initiation and growth of such wurtzite inclusions.

We have used four main techniques to characterise the quality of zinc-blende GaN layers – RHEED, photoluminescence, nuclear magnetic resonance (NMR) and X-ray diffraction. PL is very sensitive to existence of any hexagonal inclusions in the cubic GaN layers. Even minimal incorporation of wider band gap ( $\sim 3.4 \text{ eV}$ ) wurtzite GaN phase into a narrower zinc-blende GaN ( $\sim 3.2 \text{ eV}$ ) results in very strong hexagonal PL and suppression of cubic PL, probably due to high crystalline quality of direct band-gap hexagonal inclusions.

In XRD the main peak for cubic (001) GaN in a  $2\theta$ - $\omega$  scan is at  $\sim 40^\circ$ . There is no overlap of this peak with any peaks for hexagonal GaN, so we can use  $2\theta$ - $\omega$  scan as a method to study cubic inclusions in hexagonal GaN matrix. However, this is not the case for hexagonal inclusions in a cubic GaN matrix [37–39]. The position of the main 0002 peak for hexagonal GaN in  $2\theta$ - $\omega$  scan is at  $2\theta$  about  $\sim 35^\circ$ , which coincides with the 111 peak for cubic GaN in a  $2\theta$ - $\omega$  scan. We know that we have a high density of the stacking faults in cubic GaN layers and if we have a peak at  $\sim 35^\circ$  it can mean that we are looking at cubic (111) grains. Therefore, an XRD  $2\theta$ - $\omega$  scan is not a very accurate way to determine whether we have hexagonal inclusions in cubic (001) GaN layers. For GaN grown on (001) oriented GaAs, with no XRD GaN related peak at  $\sim 35^\circ$  in a  $2\theta$ - $\omega$  scan, we can conclude that we have no hexagonal inclusions oriented with the [0001] direction perpendicular to the growth surface or cubic inclusions with the [111] direction perpendicular to the same growth surface. However, this does not exclude the possibility of hexagonal inclusions growing parallel to the

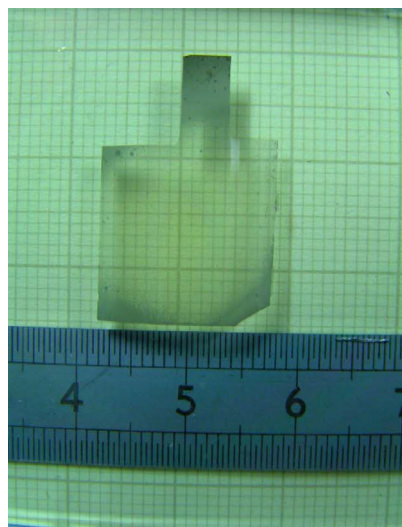


Fig. 3.. Free-standing zinc-blende GaN layers with the different thickness – (a)  $\sim 8 \mu\text{m}$  and (b)  $\sim 30 \mu\text{m}$  [33].

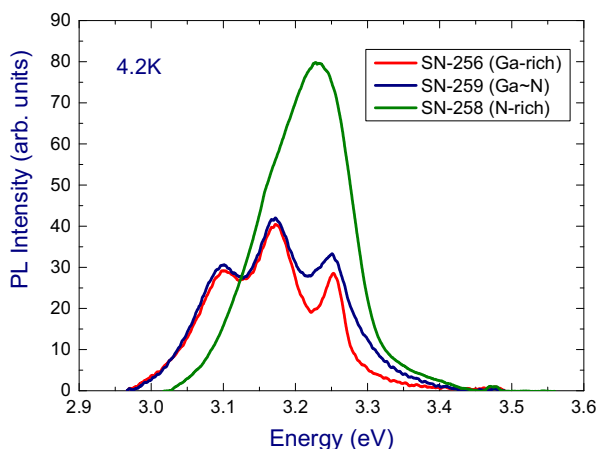


Fig. 4.. Low temperature PL data for zinc-blende GaN grown with N-rich, Ga-rich and close to stoichiometry growth conditions.

[111] direction of the cubic GaN.

It is now well established that there are 3 main growth conditions for PA-MBE of wurtzite GaN [40]. They are N-rich growth (where the active nitrogen flux is larger than the Ga-flux); Ga-rich growth (here the active nitrogen flux is less than the Ga-flux) and strongly Ga-rich growth (here the active nitrogen flux is much less than the Ga-flux and Ga droplets are formed on the surface). In our research we have established that the best structural properties of free-standing zinc-blende (cubic) GaN can be achieved with initiation under Ga-rich conditions, but before the formation of Ga droplets.

Fig. 4 shows low temperature PL spectra for three zinc-blende GaN layers grown under Ga-rich, N-rich and intermediate conditions on 2-inch GaAs substrates. We observed PL peaks attributed in the literature to excitonic recombination ( $\sim 3.25\text{--}3.27$  eV), donor-acceptor pair transitions ( $\sim 3.15\text{--}3.18$  eV) and a free to bound transition ( $\sim 3.1$  eV) in cubic GaN [31–34]. There is no indication of a hexagonal peak, expected at  $\sim 3.4$  eV. The observation of the three well resolved peaks in low temperature PL spectra is a signature of high quality zinc-blende GaN layers [41–43]. From Fig. 4 we can conclude that the best quality layers have been grown under slightly Ga-rich conditions.

Fig. 5 shows X-ray data for a cubic GaN layer  $\sim 12$   $\mu\text{m}$  thick, grown for 24 hours on a 2-inch GaAs substrate. In the figure we present the X-ray results from the as grown GaN sample on the GaAs substrate and for the free-standing GaN layer. At a GaN thickness of  $\sim 12$   $\mu\text{m}$  we were able to obtain free-standing GaN by chemically removing GaAs substrate. Both spectra show that the layer is zinc-blende GaN. The fact that we can see GaAs peaks in the GaN spectrum on the GaAs

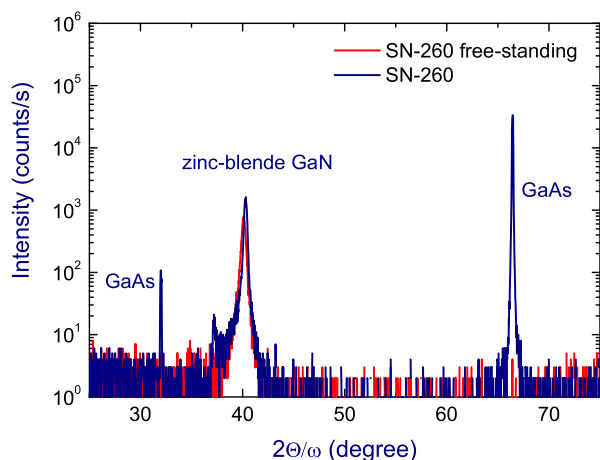


Fig. 5.. X-ray data for a zinc-blende GaN layer  $\sim 12$   $\mu\text{m}$  thick before and after removal of the GaAs substrate.



Fig. 6.. A 100  $\mu\text{m}$  thick zinc-blende GaN layer grown on a 3-inch GaAs substrate.

substrate shows that the penetration depth of XRD is more than 12  $\mu\text{m}$  and we are collecting data from the whole depth of the GaN layer. We can just see the appearance of a very small peak at  $2\theta \sim 35^\circ$ , this may be the sign of hexagonal inclusions, but may result from the formation of (111) cubic GaN stacking faults. The intensity of this peak is  $\sim 3$  orders of magnitude lower than the intensity of zinc-blende peak

To grow cubic GaN layers with a thickness  $\sim 30\text{--}100$   $\mu\text{m}$ , which is the desirable thickness for potential substrate applications, we need to grow for about 100–200 h or 4–8 days. In order to grow high quality free-standing cubic III-N layers we need, therefore, to be able to maintain the same MBE growth conditions for about one week. The free-standing cubic GaN layer shown in Fig. 6 was grown at a growth rate  $\sim 0.45$   $\mu\text{m}/\text{h}$ . There are several potential problems in achieving this, such as: 1) drift of the Ga flux due to depletion of the Ga cell; 2) drift of the active nitrogen flux due to changing the efficiency of the N plasma source during prolong operations; and 3) a slow drift of the growth temperature due to a gradual change in the emissivity of the GaAs-substrate/GaN-layer. The window for the optimum growth conditions for epitaxy of cubic GaN is not wide as can be seen from PL in Fig. 4. Therefore, each long growth requires re-calibration of the MBE system and growth of several thin GaN calibration samples.

It is difficult to maintain the optimised growth conditions for a period of several days. As a result we have observed the formation of hexagonal inclusions in GaN layers grown for more than  $\sim 24$  h and the amount of them increases with increasing GaN thickness. We have shown by several methods, including nuclear magnetic resonance (NMR) studies (Please see details in Section 1.5), that it is possible to grow zinc-blende GaN with a thickness up to 30–50  $\mu\text{m}$  with less than 10% of hexagonal phase in the best samples [33].

At present, we cannot quantify the density of wurtzite inclusions using with X-ray diffraction or transmission electron microscopy (TEM). In XRD pole plots we can see that they exist within our zinc-blende samples after a certain thickness of GaN layers. We also can see that the density of hexagonal inclusions increases with layer thickness from the increase in the intensity of the hexagonal XRD signal. The intensity of the hexagonal peaks in pole plots always remains weaker than intensity of the zinc-blende XRD peak. However, at present we are not able to quantify the density of such hexagonal inclusions as a function of thickness using XRD, because there is no simple way to translate from the intensity of the XRD hexagonal peaks in pole plots to the density of hexagonal inclusions. From NMR studies we can see that we have  $\sim 10\%$  of hexagonal phase for the  $\sim 50$   $\mu\text{m}$  thick zinc-blende layers, so this can be used as a calibration point for the XRD data. In principle, we could obtain information about hexagonal inclusions from cross-sectional TEM studies, but this would involve taking slices from different depths in the thick films and such studies have not so far been done.

However, the best quality of zinc-blende phase GaN was observed in layers less than 10  $\mu\text{m}$  thick. Micro-PL measurements indicate that the density of hexagonal inclusions increases after the first 10  $\mu\text{m}$  of growth [44]. We have recorded the PL spectra from the cleaved edge of a thick zinc-blende GaN layer as a function of the distance from the GaN/GaAs interface using a micro-PL. The PL peak intensity of hexagonal GaN ( $\sim 3.4$  eV) increases with distance from the GaN/GaAs interface. The data from NMR measurements (see Section 1.5) found that the average hexagonal content of a similar thick zinc-blende GaN layer is  $\sim 10\%$ . We used this result to estimate the approximate percentage of hexagonal inclusions in the sample as a function of thickness [44]. We found that the volume of hexagonal inclusions is  $\sim 1\%$  within 10  $\mu\text{m}$  from the GaN/GaAs interface, which would therefore appear to be the best surface to use as a template for further growth of zinc-blende GaN device structures. It is worth noting that the hexagonal fraction is still less than 20%, even near to the surface of  $\sim 50$   $\mu\text{m}$  thick zinc-blende GaN layer. Therefore, if we want to produce zinc-blende GaN substrates from our thick GaN layers it is logical to use the side of the GaN crystal that was in contact with the GaAs substrate as the epi-side surface of the future cubic GaN substrate fabrication.

Fig. 7 shows an AFM image of the surface of a free-standing zinc-blende GaN layer  $\sim 50$   $\mu\text{m}$  thick, chemically removed from the GaAs substrate. This is the surface of the GaN layer, which was previously attached to GaAs substrate. The surface is very smooth and has an RMS roughness of  $\sim 0.7$  nm.

### 1.2. Arsenic impurities in the zinc-blende GaN layers

Our process requires growth of GaN for several days, during which time the GaAs substrate is maintained at a high temperature of  $\sim 700$   $^{\circ}\text{C}$ , potentially resulting in unintentional As doping of the GaN layer due to diffusion. Arsenic contamination is not desirable for the epi-ready surface of zinc-blende GaN substrates and therefore this part needs to be removed by polishing. The aim of the current section is to discuss arsenic incorporation into zinc-blende (001) GaN during the initiation phase of the epitaxy and during further long MBE growths.

In the secondary ion mass spectrometry (SIMS) studies of the thin zinc-blende GaN layers ( $< 5$   $\mu\text{m}$ ) we were able to sputter through the GaN layer into the GaAs substrate [45]. We have used calibration standards for As in GaN in order to quantify the As concentrations in our layers. Fig. 8 shows the arsenic and nitrogen profiles in a relatively thin zinc-blende GaN layer from the surface down to the interface with GaAs. The arsenic concentration drops abruptly at the interface from the bulk value for GaAs to the background value of SIMS system at  $\sim 10^{18}$   $\text{cm}^{-3}$  inside the GaN. Sputtering rate changes were employed to

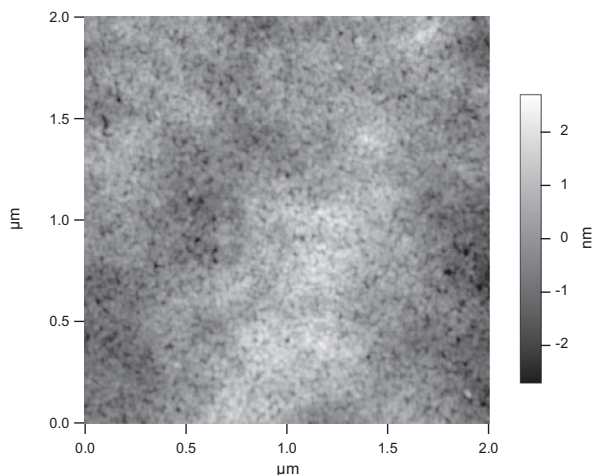


Fig. 7.. An AFM image for a 50  $\mu\text{m}$  thick zinc-blende GaN layer after removal of the GaAs substrate [37].

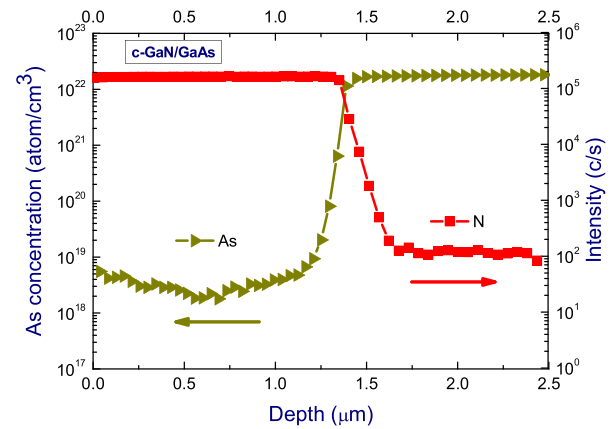


Fig. 8.. The As and N profiles measured by SIMS in thin zinc-blende GaN layers grown on GaAs.

determine the instrumental backgrounds of the SIMS systems and for As the measured background is  $\sim (7-8) 10^{17}$   $\text{cm}^{-3}$  in both Cameca systems used for the SIMS measurements. From Fig. 8 we can conclude that any significant arsenic contamination is limited to the first  $\sim 200$  nm of the zinc-blende GaN layer. However, noting that the abrupt change in the nitrogen signal at the interface covers a similar depth to that for the arsenic it can suggest that the real depth of any arsenic contamination is likely to be even lower, due to roughening during the SIMS measurements.

For the thicker layers (5–100  $\mu\text{m}$  range), SIMS sputtering through the whole GaN is not viable. We were able to obtain free-standing zinc-blende GaN layers, which allowed us to perform SIMS studies on both sides of the free-standing GaN layers. The arsenic profiles for the samples with significantly different growth times were practically identical [45], which demonstrates that there is no significant diffusion of As into GaN during prolonged MBE growths. The depth of the As incorporation did not change significantly with increasing growth time from a few hours to a few days. Therefore, we can conclude that arsenic incorporation is limited to the first few hundred nanometers of the GaN layer and it is due to the initiation phase of the growth of zinc-blende material, which involves use of arsenic as a surfactant to promote the growth of the cubic phase.

We have developed a process to remove the thin ( $< 1$   $\mu\text{m}$ ), lightly As contaminated, region of GaN using a standard polishing process. We are able to maintain the mirror like surface after polishing with measured by AFM RMS roughness of  $\sim 0.7$  nm, values similar to that of the original surface. We have developed a procedure to cleave the wafers into the shape and size required for further processing to produce free-standing zinc-blende GaN substrates, as shown in Fig. 9.

### 1.3. Doping of free-standing zinc-blende GaN layers

In this part we discuss the results on n- and p-doping of free-standing zinc-blende GaN grown by PA-MBE. We use Si as the n-type dopant and Mg as the p-type dopant for zinc-blende GaN [46,47].

Fig. 10 shows a SIMS profiles for Si at the centre of an GaN: Si layer with a thickness  $\sim 6$   $\mu\text{m}$ . The position of the GaN/GaAs interface is clearly marked by the spike in Si incorporation and the Si incorporation is uniform through the Si-doped part of the GaN layer. With increasing Si cell temperature we observe in SIMS an increase in the Si doping level. All Si-doped GaN layers have n-type conductivity according to both thermopower studies and Hall measurements. For the thin GaN: Si layers we have good agreement between Hall measurements of the carrier concentrations and SIMS data for the Si level. PL of thin and free-standing zinc-blende GaN: Si layers have been studied [47]. In the low temperature PL spectra of zinc-blende GaN: Si we observed an excitonic recombination related peak at  $\sim 3.3$  eV and a donor-acceptor

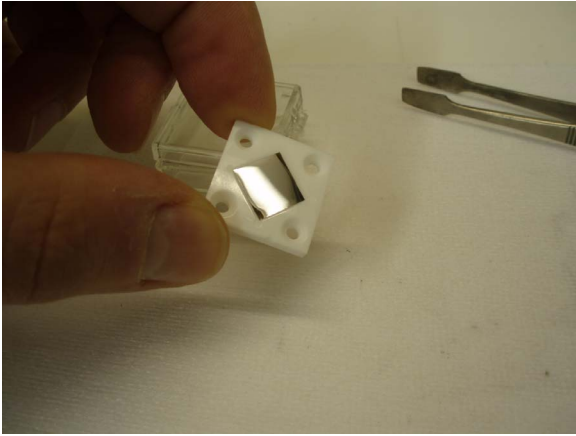


Fig. 9.. A  $10 \times 10 \text{ mm}^2$  zinc-blende free-standing GaN substrate prepared for further epitaxy.

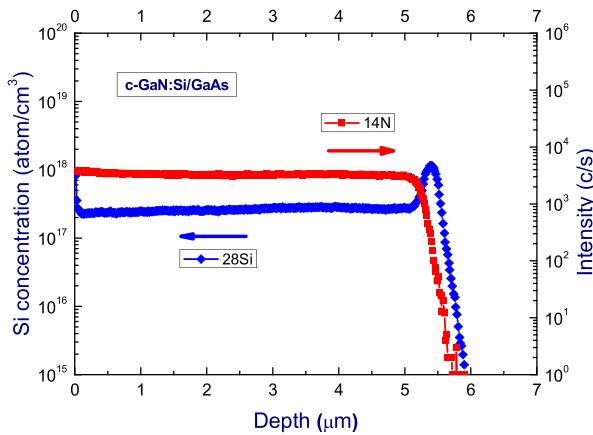


Fig. 10.. SIMS profiles for Si and N at the centre of  $\sim 6 \mu\text{m}$  thick zinc-blende GaN:Si layer.

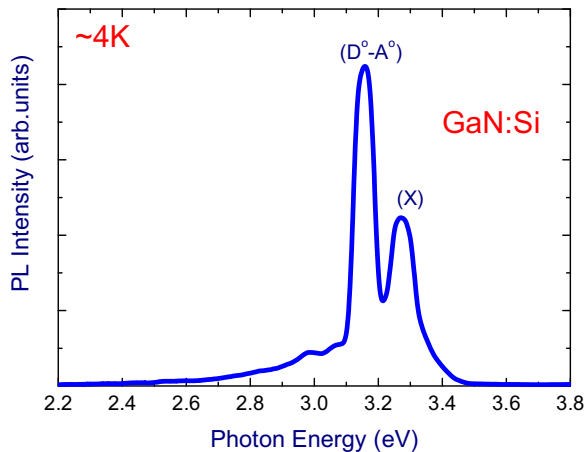


Fig. 11.. Low temperature photoluminescence from a Si doped zinc-blende GaN.

peak at  $\sim 3.15 \text{ eV}$ , as shown in Fig. 11. This data agrees with the previously published results for the thin zinc-blende GaN: Si layers [48].

Magnesium (Mg) was used as a potential p-dopant for free-standing zinc-blende GaN. Again, initially we developed p-doping of the thin zinc-blende layers GaN grown by MBE over a wide range of the Mg concentrations. We did not observe any difference in SIMS profiles for the distribution of  $^{24}\text{Mg}$  and  $^{25}\text{Mg}$  isotopes of magnesium [46]. The Mg incorporation is uniform through the Mg-doped part of the GaN layer.

The PL spectra for our zinc-blende GaN:Mg samples are consistent with other studies of the thin Mg-doped zinc-blende GaN [48]. Fig. 12

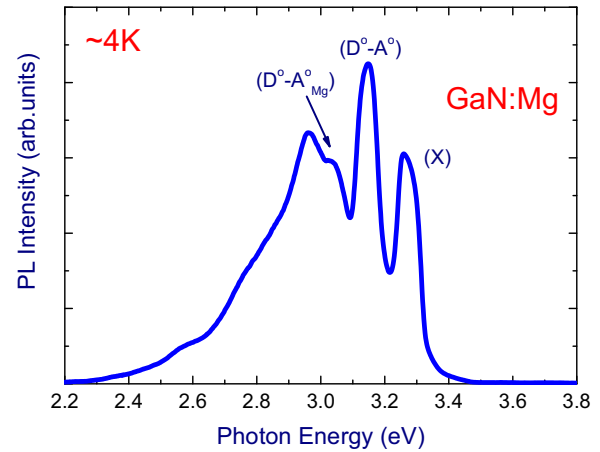


Fig. 12.. Low temperature photoluminescence from a Mg-doped zinc-blende GaN layer.

shows that we observed PL peaks corresponding to impurity bound excitonic transitions at  $3.15 \text{ eV}$ , the donor-acceptor recombination at  $3.25 \text{ eV}$ , and transitions involving a shallow Mg acceptor at  $3.05 \text{ eV}$  [47].

Therefore, controllable n- and p-doping of free-standing zinc-blende GaN using Si and Mg by PA-MBE can be achieved. The fact that n- and p-doped free-standing zinc-blende GaN wafers can be grown by PA-MBE opens the possibility of the future production of n- and p-doped free-standing zinc-blende GaN for vertical device structures.

#### 1.4. MBE of InGaN LEDs structures on free-standing zinc-blende GaN substrates

In order to test the feasibility of using such free-standing zinc-blende GaN layers as a substrate for the further epitaxy of zinc-blende device structures we have provided our layers to Sharp Laboratories of Europe (SLE). We have supplied SLE with free-standing GaN with thicknesses in the range  $50$  to  $100 \mu\text{m}$  and size  $10 \times 10 \text{ mm}^2$ . As has been discussed in Section 1.2, we have developed a polishing process to remove the thin, lightly As contaminated, region of GaN. Therefore, we have provided SLE with polished and with unpolished free-standing zinc-blende GaN. Our collaborators at SLE have used their standard recipes to grow LEDs structures on our free-standing GaN wafers.

GaN-InGaN p-i-n structures were grown by MBE at SLE on our free-standing zinc-blende GaN substrates [49]. The device structure is shown in Fig. 13. It consists of a  $500 \text{ nm}$  thick Si-doped GaN buffer layer followed by a  $30 \text{ nm}$  thick InGaN active layer with  $\sim 10\%$  In concentration. Above InGaN layer we have a  $\sim 3 \text{ nm}$  thick undoped GaN and a  $400 \text{ nm}$  thick layer of Mg-doped GaN at the top of the structure. Contacts were made to the n and p type regions using In and Ni/Au layers respectively.

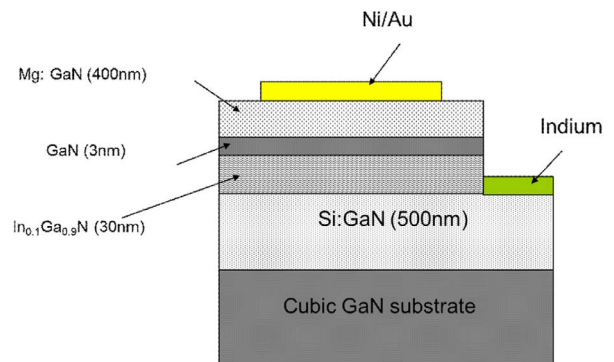


Fig. 13.. The structure of the zinc-blende InGaN LED grown on the free-standing zinc-blende GaN.

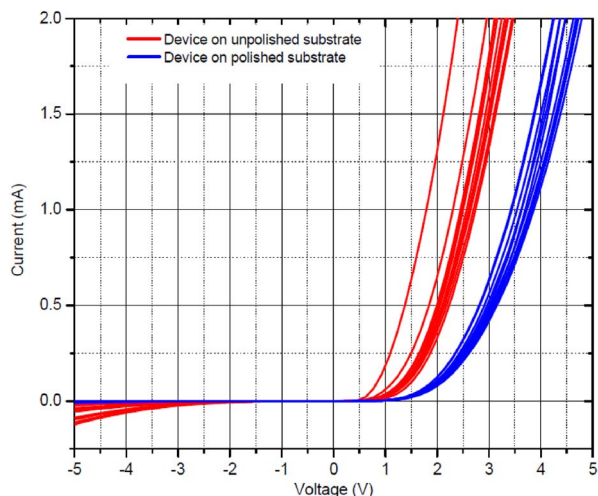


Fig. 14.. I-V characteristic of the zinc-blende InGaN LED grown on free-standing GaN .

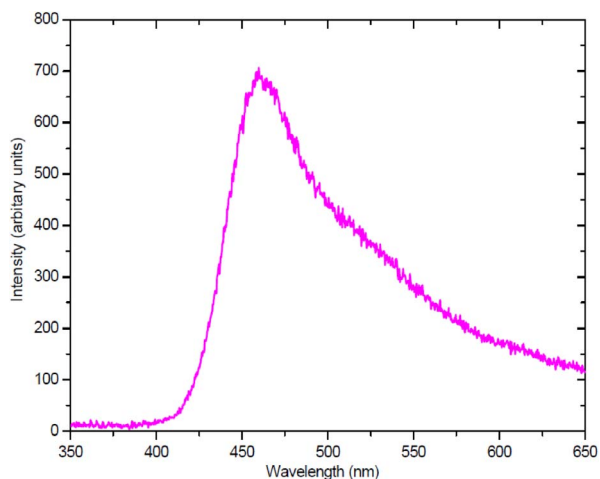


Fig. 15.. The electroluminescence spectrum for the InGaN LED under forward bias.

Fig. 14 shows the I-V characteristics of the InGaN LED device produced at SLE by MBE on our free-standing zinc-blende GaN substrates. The turn-on voltage of the devices is better for LEDs structures grown on polished GaN wafers and improved from  $\sim 2$  V to 4 V. Fig. 15 shows the resulting spectral characteristics of the zinc-blende InGaN LED with a peak emission at room temperature of  $\sim 460$  nm, significantly red-shifted from pure GaN.

These preliminary results confirm that our free-standing zinc-blende GaN wafers with thicknesses in the range 50 to 100  $\mu\text{m}$  can be used as substrates for the growth of working InGaN LEDs structures.

### 1.5. MBE of zinc-blende GaN layers with $^{15}\text{N}$ isotope gas for NMR applications

Nuclear magnetic resonance (NMR) is a powerful tool for chemical and structural analysis. The technique suffers from low sensitivity due to the small thermal equilibrium values of the nuclear magnetic polarization, however, the sensitivity can be improved by “hyperpolarizing” the nuclei. Previously it has been demonstrated that by optical pumping zinc-blende semiconductors, e.g. GaAs and InP, with circular polarized band gap radiation it is possible to hyperpolarize the nuclear spins ( $^{71}\text{Ga}$  and  $^{31}\text{P}$ ) [50–52]. The optical pumping excites spin polarized electrons which transfer their polarization to the nuclei by Overhauser cross relaxation processes. The non-thermal spin populations produced in this way can give rise to an increased NMR signal. Using a technique known as transferred optically pumped NMR

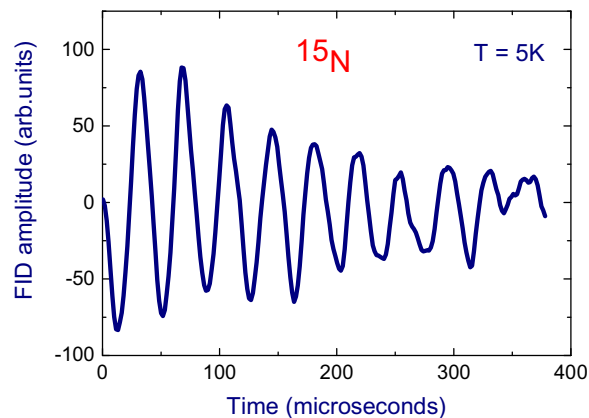


Fig. 16.. Free induction decay from  $^{15}\text{N}$  in zinc-blende GaN, NMR frequency 20 MHz.

(TOPNMR), the polarization in the semiconductor can be transferred to a material on the surface. In this way, enhanced NMR signals can be obtained from very small amounts of, for example, a biological sample. Owing to its high chemical stability, GaN would appear to be an ideal material for use in TOPNMR. Furthermore, it can be grown by PA-MBE using  $^{15}\text{N}$  isotope nitrogen gas. The  $^{15}\text{N}$  nucleus is spin 1/2 and, unlike  $^{71}\text{Ga}$ , it does not suffer from quadrupole effects, which can act as a barrier to spin exchange at the semiconductor surface.

We have demonstrated the PA-MBE growth of zinc-blende GaN films using high-purity  $^{15}\text{N}$  isotope gas as a nitrogen source [53]. We have detected the NMR signal from the  $^{15}\text{N}$  in a powdered sample of  $\text{Ga}^{15}\text{N}$  at 20 MHz ( $\sim 5$  T field), shown in Fig. 16. It was possible to use the NMR results to estimate the hexagonal GaN fraction in the measured samples: the different crystal fields associated with the zinc-blende and wurtzite phases give rise to different relaxation times which can be resolved in the measurements [33]. We also observed enhancement of the  $^{15}\text{N}$  nuclear polarization in zinc-blende  $\text{Ga}^{15}\text{N}$  by pumping the sample with circular-polarized UV light. A maximum enhancement of  $\sim 30\%$  was measured, which is small compared to the enhancements previously observed in GaAs and InP. We believe this is due to the high background carrier concentration in this particular GaN sample. Further work is underway to produce compensated material, which should exhibit larger polarization enhancement under optical pumping.

### 1.6. MBE of free-standing zinc-blende AlGaIn layers

We have demonstrated that our newly developed PA-MBE process for the growth of thick zinc-blende GaN layers also allows us to achieve free-standing ternary  $\text{Al}_x\text{Ga}_{1-x}\text{N}$  wafers [54]. Zinc-blende  $\text{Al}_x\text{Ga}_{1-x}\text{N}$  films were grown on 2-inch and 3-inch diameter semi-insulating GaAs (001) substrates.

Initially we developed MBE growth of thin zinc-blende  $\text{Al}_x\text{Ga}_{1-x}\text{N}$  layers for the complete Al composition range  $x$  from 0 to  $\sim 1$ . We have grown zinc-blende  $\text{Al}_x\text{Ga}_{1-x}\text{N}$  layers on GaAs substrates and used thin ( $\sim 75$  nm) zinc-blende GaN buffers to initiate the growth of the zinc-blende phase. The quality of  $\text{Al}_x\text{Ga}_{1-x}\text{N}$  layers degrades with increasing Al content. In order to sustain the cubic phase during epitaxy it is crucial to maintain an excess of group III elements on the growth surface. It is well established that exposing a c-AlN surface to nitrogen flux leads to the formation of hexagonal AlN clusters [20,55]. We have used a new approach to maintain an excess of group III elements for the growth of  $\text{Al}_x\text{Ga}_{1-x}\text{N}$  layers for a wide Al composition range. We have used an excess Ga flux. The energy of the Al-N bond is significantly stronger than the energy of Ga-N bond. Therefore, we observed preferential incorporation of Al into the  $\text{Al}_x\text{Ga}_{1-x}\text{N}$  layers from the Ga-Al liquid on the surface. This method allows us to sustain zinc-blende growth of  $\text{Al}_x\text{Ga}_{1-x}\text{N}$  layers over almost the whole Al composition range. The only disadvantage of this approach is that excess Ga is

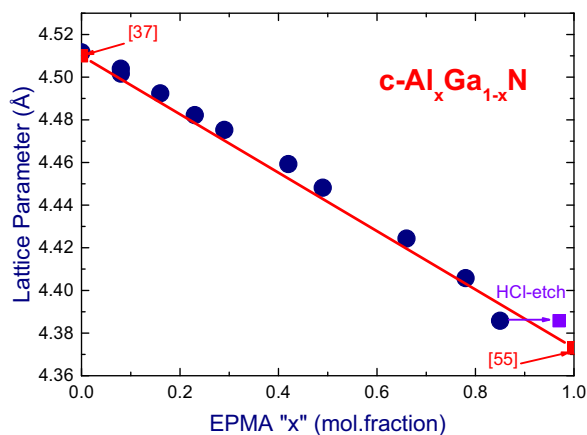


Fig. 17.. Dependence of lattice parameter on composition for zinc-blende  $\text{Al}_x\text{Ga}_{1-x}\text{N}$  layers grown by PA-MBE.

present on the surface after growth and forms Ga-rich droplets. However, these Ga droplets can be chemically removed after growth.

There is a measurable difference in the lattice parameters of GaN and AlN and, therefore, in a  $2\theta$ - $\omega$  scan we have observed a monotonic shift of the zinc-blende XRD peak for the  $\text{Al}_x\text{Ga}_{1-x}\text{N}$  layers with increasing Al content. From the position of the XRD peak we were able to estimate the lattice parameter of the  $\text{Al}_x\text{Ga}_{1-x}\text{N}$  layers. The Al content in each  $\text{Al}_x\text{Ga}_{1-x}\text{N}$  layer were measured using electron probe micro-analysis (EPMA). Fig. 17 shows the dependence of the lattice parameter of zinc-blende  $\text{Al}_x\text{Ga}_{1-x}\text{N}$  layer as a function of the Al content in the layer, measured by EPMA. The Ga excess on the surface of the  $\text{Al}_x\text{Ga}_{1-x}\text{N}$  layers may cause uncertainty in the EPMA measurements of the composition. Therefore, we have chemically removed the Ga from the surface of  $\text{Al}_x\text{Ga}_{1-x}\text{N}$  layers with a high Al content before the EPMA measurements, as shown in Fig. 17.

In the same Fig. 17, we also plot a linear extrapolation from the values of lattice parameters for GaN and AlN. For the GaN we have used our value measured for the free-standing zinc-blende GaN [37] and for the AlN we have used the value for the thin c-AlN layers grown on 3C-SiC [55]. The lattice parameter of thin cubic  $\text{Al}_x\text{Ga}_{1-x}\text{N}$  layers changes almost linearly from the value for the cubic GaN to the value for AlN and thus closely follows Vegard's law.

Fig. 18 shows the dependence of the photon energy  $E_{\text{PL}}^{\text{max}}$  on the composition of zinc-blende  $\text{Al}_x\text{Ga}_{1-x}\text{N}$  layers. The increase of  $E_{\text{PL}}^{\text{max}}$  with the increase of AlN content is in qualitative agreement with the increase of the bandgap  $E_g$  [56]. However, the values for  $E_g$  and its direct or indirect origin in zinc-blende  $\text{Al}_x\text{Ga}_{1-x}\text{N}$  alloys are still under debate [20,57,58]. In analogy with hexagonal  $\text{Al}_x\text{Ga}_{1-x}\text{N}$  [59] we may expect that the Stokes shift for the PL peak relative to  $E_g$  at high AlN

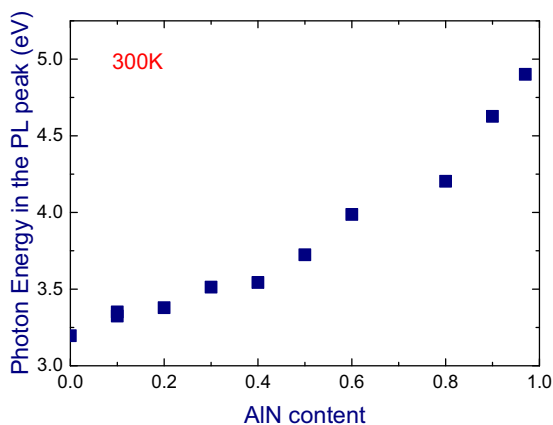


Fig. 18.. The dependence of the photon energy at the maximum of the PL intensity for zinc-blende  $\text{Al}_x\text{Ga}_{1-x}\text{N}$  layers on the AlN content.

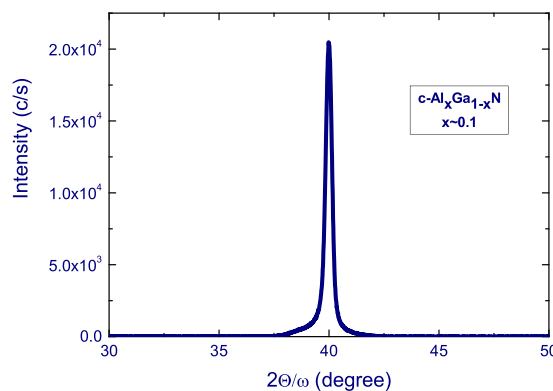


Fig. 19.. XRD data at the centre of 2-inch diameter free-standing zinc-blende  $\text{Al}_x\text{Ga}_{1-x}\text{N}$  wafer with  $x \sim 0.1$  and with a thickness of  $\sim 10 \mu\text{m}$ .

content is more than 100 meV due to localization effects and electron-phonon interactions [60] in the studied samples.

We have shown that photoexcited electrons and holes in zinc-blende  $\text{Al}_x\text{Ga}_{1-x}\text{N}$  alloys at  $x > 0.5$  possess strong localization at room temperature. As a result, the intensity of the near-band edge PL increases by more than two orders of magnitude in comparison with pure zinc-blende GaN. The activation energy for localized carriers increases linearly with AlN content, and at  $x = 0.95$ , it reaches the value of 55 meV [56]. The decay of PL from localized carriers is non-exponential due to the spatial separation of electrons and holes.

Based on the results for the thin  $\text{Al}_x\text{Ga}_{1-x}\text{N}$  layers, we have developed MBE growth of free-standing zinc-blende  $\text{Al}_x\text{Ga}_{1-x}\text{N}$  layers with an AlN content  $x$  from 0 up to close to 1. We have grown them on GaAs substrates and subsequently removed the GaAs in order to achieve free-standing  $\text{Al}_x\text{Ga}_{1-x}\text{N}$  wafers. Fig. 19 presents XRD data from a free-standing  $\text{Al}_x\text{Ga}_{1-x}\text{N}$  wafer with a composition of  $x \sim 0.10$  and a thickness of  $\sim 10 \mu\text{m}$ . XRD shows only a single peak at  $\sim 40^\circ$ , which is the correct position of the peak for zinc-blende  $\text{Al}_x\text{Ga}_{1-x}\text{N}$ .

We have studied Al incorporation in the layers using SIMS and EPMA [54]. We were able to obtain free-standing zinc-blende  $\text{Al}_x\text{Ga}_{1-x}\text{N}$  layers, which allowed us to perform SIMS studies on both sides of the free-standing layers. In SIMS we observed a uniform distribution of Al, Ga and N within the bulk of the  $\text{Al}_x\text{Ga}_{1-x}\text{N}$  layers. There is no significant As incorporation into the bulk of  $\text{Al}_x\text{Ga}_{1-x}\text{N}$  layers, which was confirmed by the As signal being at the background level of the SIMS system. Therefore, the MBE method we have developed allows us to achieve the growth of free-standing  $\text{Al}_x\text{Ga}_{1-x}\text{N}$  crystals with a constant composition.

These SIMS results are also confirmed by EPMA measurements on a free-standing  $\text{Al}_x\text{Ga}_{1-x}\text{N}$  2-inch diameter layer as shown in Fig. 20. Quantitative analysis was performed along a diameter of the 2-inch diameter free-standing wafer on the side previously in contact with the GaAs substrate using 10 keV electrons, which penetrate approximately 650 nm into the layer. Averaging sixteen data points gave a AlN mole fraction of 8.3%. Fig. 20 shows that the distribution of all elements to be very uniform and the arsenic concentration inside the layer is at or below the detection limit ( $\sim 5 \cdot 10^{18} \text{ cm}^{-3}$ ) of the EPMA system.

However, with increasing Al concentration the Al distribution becomes less uniform, with the minimum Al content close to the centre of the wafer. We can attribute this effect to the strong dependence of the Al incorporation on the group III:N ratio during the PA-MBE under Ga-rich conditions. It is well established in the PA-MBE growth of hexagonal  $\text{Al}_x\text{Ga}_{1-x}\text{N}$  layers that under the Ga-rich conditions of the growth the Al fraction increases with decreasing N flux due to preferential incorporation of the Al over Ga [61,62]. In our case we have slightly more N-rich conditions in the centre of the wafer. We are now investigating ways of minimising this effect.

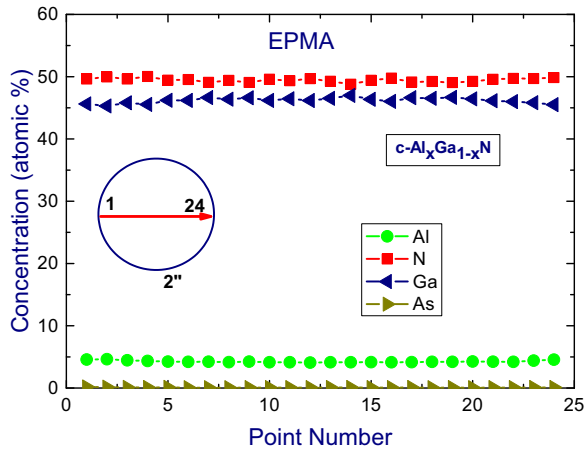


Fig. 20.. EPMA data on the lateral distribution of the As, Ga, Al and N on the surface of a free-standing 2-inch diameter zinc-blende  $\text{Al}_x\text{Ga}_{1-x}\text{N}$  layer.

### 1.7. MBE of free-standing wurtzite $\text{Al}_x\text{Ga}_{1-x}\text{N}$ layers

Free-standing wurtzite (hexagonal)  $\text{Al}_x\text{Ga}_{1-x}\text{N}$  films can be also grown on by our PA-MBE method [63,64]. We have grown layers on (111)B oriented GaAs substrates in order to initiate the epitaxy of hexagonal  $\text{Al}_x\text{Ga}_{1-x}\text{N}$  layers.

Initially we have performed PA-MBE growth of thin wurtzite  $\text{Al}_x\text{Ga}_{1-x}\text{N}$  layers on (111)B GaAs substrates for Al compositions ranging from 0 up to 0.5. As expected, in  $2\theta$ - $\omega$  XRD plots with increasing Al content in the layers we observed a gradual shift of the position of the  $\text{Al}_x\text{Ga}_{1-x}\text{N}$  XRD peak to higher angle. PL and CL studies have confirmed an increase of the band gap of  $\text{Al}_x\text{Ga}_{1-x}\text{N}$  layers with increasing Al content.

Based on these results we have grown  $\sim 10\ \mu\text{m}$  thick wurtzite  $\text{Al}_x\text{Ga}_{1-x}\text{N}$  layers under the similar growth conditions with  $x$  from 0 up to 0.5. From our previous experience with MBE growth of zinc-blende GaN, such a thickness is already enough to obtain free-standing  $\text{Al}_x\text{Ga}_{1-x}\text{N}$  layers without cracking and at the same time does not require very long growth runs. To increase the thickness even further to 50–100  $\mu\text{m}$  is merely a technical task as we have shown earlier for cubic AlGaN. For this demonstration of the feasibility of the method, therefore, we have chosen to grow all  $\text{Al}_x\text{Ga}_{1-x}\text{N}$  layers up to a thickness of  $\sim 10\ \mu\text{m}$ .

Fig. 21 shows a  $2\theta$ - $\omega$  XRD plot for a  $10\ \mu\text{m}$  thick free-standing  $\text{Al}_x\text{Ga}_{1-x}\text{N}$  layer. In XRD studies we have observed a single peak at  $\sim 35^\circ$ , which is the correct position for a wurtzite  $\text{Al}_x\text{Ga}_{1-x}\text{N}$  layer. Using Vegard's law, we can estimate the composition of the  $\text{Al}_x\text{Ga}_{1-x}\text{N}$  layer shown in Fig. 21 to be  $x \sim 0.25$ . The value of AlN content in this

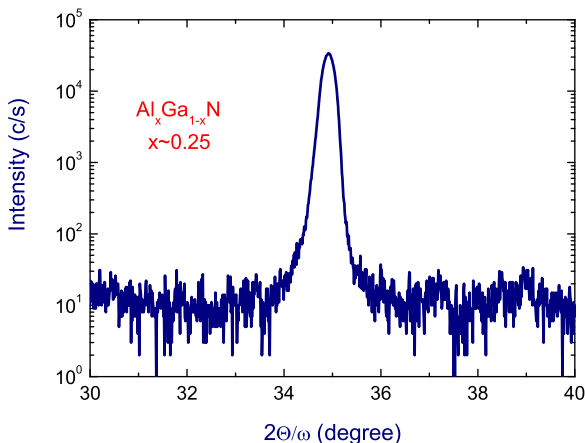


Fig. 21.. A  $2\theta$ - $\omega$  XRD plot for a  $10\ \mu\text{m}$  thick free-standing wurtzite  $\text{Al}_x\text{Ga}_{1-x}\text{N}$  layer with  $x \sim 0.25$ .

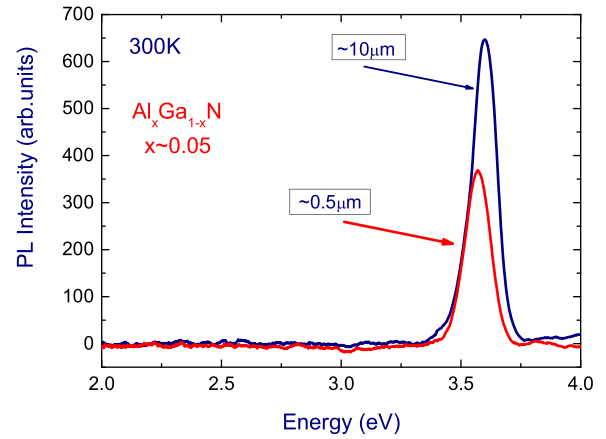


Fig. 22.. Room temperature PL from the surfaces of the thin ( $\sim 0.5\ \mu\text{m}$ ) and thick ( $\sim 10\ \mu\text{m}$ )  $\text{Al}_x\text{Ga}_{1-x}\text{N}$  layers with  $x \sim 0.05$ .

$\text{Al}_x\text{Ga}_{1-x}\text{N}$  layer was confirmed by EPMA measurements. As we have previously shown, from high resolution XRD scans we can estimate the zinc-blende fraction, which in this case was below our detection limit ( $< 0.1\%$ ).

Fig. 22 shows room temperature PL from the surfaces of the thin ( $\sim 0.5\ \mu\text{m}$ ) and thick ( $\sim 10\ \mu\text{m}$ )  $\text{Al}_x\text{Ga}_{1-x}\text{N}$  layers with  $x \sim 0.05$ . Both  $\text{Al}_x\text{Ga}_{1-x}\text{N}$  layers were measured while they were still on the GaAs substrates. We can observe strong PL peaks for both thin and thick  $\text{Al}_x\text{Ga}_{1-x}\text{N}$  layers. The position of both peaks is shifted from the GaN band gap to  $\sim 3.6\ \text{eV}$ , as expected for a  $\text{Al}_x\text{Ga}_{1-x}\text{N}$  layer with  $x \sim 0.05$ . We can observe a slightly higher PL energy for the thicker  $\text{Al}_x\text{Ga}_{1-x}\text{N}$  layer, which shows that the AlN content in this sample is probably slightly higher. In both samples there is no evidence for any yellow PL band at around  $2.2\ \text{eV}$  or PL from any zinc-blende  $\text{Al}_x\text{Ga}_{1-x}\text{N}$  inclusions.

Fig. 23 shows the XRD data for four free-standing  $\text{Al}_x\text{Ga}_{1-x}\text{N}$  wafers of different composition. All four samples have a thickness of  $\sim 10\ \mu\text{m}$  and were mounted on glass with wax. The AlN content of the  $\text{Al}_x\text{Ga}_{1-x}\text{N}$  layers was estimated from the position of the XRD peak using Vegard's law and was confirmed by EPMA studies. We have grown a thin ( $\sim 50\ \text{nm}$ ) wurtzite GaN buffer layer before the growth of all  $\text{Al}_x\text{Ga}_{1-x}\text{N}$  layers and this GaN buffer can be seen as a shoulder on the XRD data in Fig. 23 for the samples with the high Al content.

From XRD data the dependence of the lattice parameters for  $\text{Al}_x\text{Ga}_{1-x}\text{N}$  were measured as a function of the AlN content and the results for c-lattice are shown in Fig. 24. The estimated  $\text{Al}_x\text{Ga}_{1-x}\text{N}$  composition data were confirmed by EPMA studies. On the figure we have also plotted c-lattice constants for GaN and AlN and a linear estimate for  $\text{Al}_x\text{Ga}_{1-x}\text{N}$  alloys c-lattice constants using Vegard's law. Fig. 24 shows that c-lattice parameter for free-standing wurtzite  $\text{Al}_x\text{Ga}_{1-x}\text{N}$  layers decreases linearly

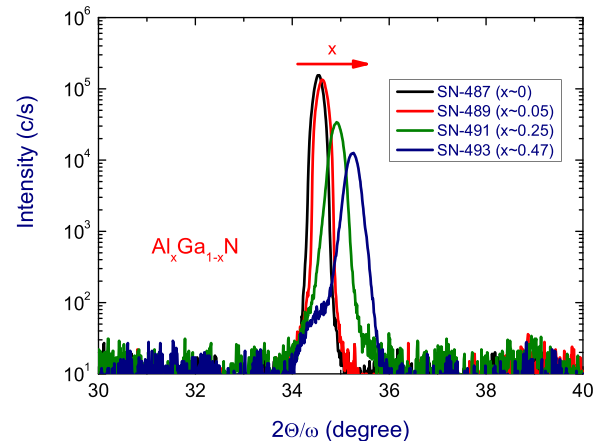


Fig. 23.. XRD data for 4 free-standing  $\text{Al}_x\text{Ga}_{1-x}\text{N}$  wafers of different composition.

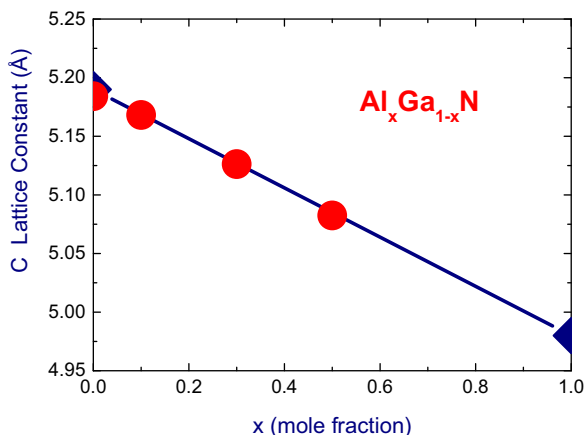


Fig. 24.. The variation in c lattice parameter for 10  $\mu\text{m}$  thick wurtzite  $\text{Al}_x\text{Ga}_{1-x}\text{N}$  layers as a function of aluminium content.

with decreasing AlN content in good agreement with Vegard's law.

In order to study the lateral distribution of the elements across the 2-inch diameter wurtzite  $\text{Al}_x\text{Ga}_{1-x}\text{N}$  wafer, we have performed EPMA studies on the surface of the  $\text{Al}_x\text{Ga}_{1-x}\text{N}$  previously attached to the GaAs substrate. Fig. 25 shows the lateral distribution of the AlN and GaN contents for the  $\sim 10 \mu\text{m}$  thick free-standing  $\text{Al}_x\text{Ga}_{1-x}\text{N}$  wafer with  $x \sim 0.5$ . Fig. 25 confirms that we were able to achieve a uniform distribution of AlN content across the diameter for the central part of the 2-inch  $\text{Al}_x\text{Ga}_{1-x}\text{N}$  wafer. However, close to the edge of the wafer the Al distribution becomes less uniform, with the maximum AlN content close to the edge, as we demonstrated previously in zinc-blende AlGaIn layers. We again attribute this effect to the strong dependence of the Al incorporation on the group III:N ratio during PA-MBE. In order to minimize this effect we will optimize the thickness of the PBN backing plates used in our PA-MBE substrate holders.

### 1.8. Increasing the MBE growth rate of free-standing wurtzite $\text{Al}_x\text{Ga}_{1-x}\text{N}$ layers

We have used the MBE technique and have produced free-standing layers of GaN and  $\text{Al}_x\text{Ga}_{1-x}\text{N}$  up to 100  $\mu\text{m}$  in thickness. However, in our studies, the growth rate for  $\text{Al}_x\text{Ga}_{1-x}\text{N}$  films remained below 1  $\mu\text{m}/\text{h}$  and this is too slow to make the process commercially viable. We need to increase the growth rate and decrease the growth time required to achieve free-standing  $\text{Al}_x\text{Ga}_{1-x}\text{N}$  layers to less than one day.

A few years ago Riber developed a novel plasma source for the fast growth of GaN layers - RF-N 50/63. Riber modified the construction of the source and optimised the design of pyrolytic boron nitride (PBN)

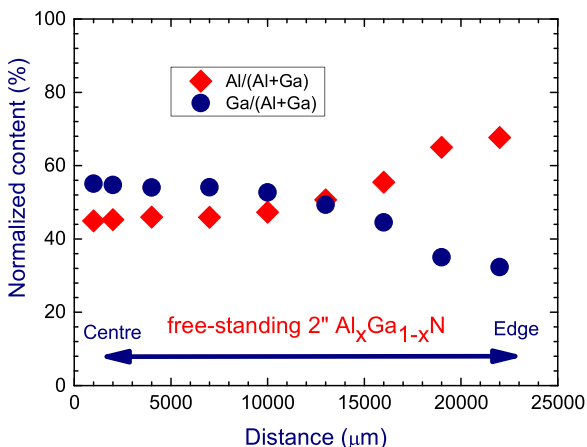


Fig. 25.. EPMA data on lateral distribution of Al and Ga on the surface of a 2-inch diameter  $\text{Al}_x\text{Ga}_{1-x}\text{N}$  layers with  $x \sim 0.5$ .

crucible and PBN aperture arrangement. The conductance of the aperture plate was increased by increasing the number of 0.3 mm diameter holes to 1200. The first tests of the novel Riber source were performed for the growth of very thin GaN layers grown for 5 min on small size wafers [66]. The authors of that work demonstrated that with this novel source it was possible to achieve GaN growth rates up to 2.65  $\mu\text{m}/\text{h}$  [66]. We have successfully used similar type Riber plasma source to demonstrate growth rates of thick GaN layers up to 1.8  $\mu\text{m}/\text{h}$  on 2-inch diameter GaAs (111)B and sapphire wafers [65].

Recently, Riber have again modified the design of the aperture of their plasma source for even faster growth of GaN layers. The aperture conductance has been increased again by increasing the number of holes, which allows a further increase in the GaN growth rate. Researchers from Santa Barbara have demonstrated that the new source with 5880 holes in the aperture plate allows them to achieve growth rates for thin GaN layers up to 7.6  $\mu\text{m}/\text{h}$  with very high nitrogen flow rates of about 25 sccm [67]. Veeco is following the same path, in their latest design they have replaced original plasma aperture with a 5.6 times higher conductance aperture in order to allow for higher gas flow while still maintaining the high-brightness RF nitrogen plasma mode [68]. First tests of the new Veeco's source demonstrated growth rates for thin GaN layers up to 9.8  $\mu\text{m}/\text{h}$ , which was achieved using 20 sccm of  $\text{N}_2$  plus 7.7 sccm Ar flows at 600 W of RF power [68].

In this section we will describe our recent results in the development of our PA-MBE approach for the growth of free-standing wurtzite  $\text{Al}_x\text{Ga}_{1-x}\text{N}$  crystals using the latest model of fast-growing Riber RF plasma source with 5880 holes in the aperture plate [69–71].

Initially we carried out PA-MBE growth of thin ( $\sim 1 \mu\text{m}$ ) wurtzite  $\text{Al}_x\text{Ga}_{1-x}\text{N}$  layers on 2-inch diameter (111)B GaAs substrates. Wurtzite GaN buffers,  $\sim 50 \text{ nm}$  thick, were deposited before the growth of all the  $\text{Al}_x\text{Ga}_{1-x}\text{N}$  layers. The HD25 plasma source from Oxford Applied Research and a modified novel high efficiency plasma source from Riber were compared for the initiation of GaN on (111)B GaAs substrates. For both RF plasma sources we observed a hexagonal GaN RHEED pattern a few minutes into the growth.

Zinc-blende crystallites have been observed at the GaN layer/GaAs (111)B substrate interface as shown in Fig. 26. Zinc-blende crystallites extend for the first few tens of nanometres into the GaN wurtzite film, before being terminated at (0001) basal plane stacking faults. A small fraction of zinc-blende GaN close to the interface may be explained by As contamination of the first nanometers of the GaN layer. We have also observed some erosion of the GaAs substrate surface. There may be two main reasons for the roughening of the GaAs interface – it may be a result of the initial N-plasma etching or it may be a result of Ga-melt etching due to the relatively high As solubility in Ga at MBE growth temperatures. We still have not resolved which of these mechanisms is dominant.

From general considerations one might expect that GaN layers grown on a GaAs (111)A surface will exhibit Ga-polarity, but N-polarity will become preferable for the growth on GaAs (111)B substrates. However, it was demonstrated that this may depend strongly on the MBE growth conditions [72].

The polarity of our  $\text{Al}_x\text{Ga}_{1-x}\text{N}$  and GaN layers grown with high growth rates have been investigated using high resolution Scanning Transmission Electron Microscopy (HR-STEM) [71]. Fig. 27 shows HR-STEM images of three areas of the GaN buffer and  $\text{Al}_x\text{Ga}_{1-x}\text{N}$  film viewed at atomic resolution. The  $\text{Al}_x\text{Ga}_{1-x}\text{N}$  film clearly shows N-polarity due to the relative positions of the individual nitrogen atomic columns with respect to the gallium atom columns in the wurtzite crystal along the [0001] direction. The polarity of the  $\text{Al}_x\text{Ga}_{1-x}\text{N}$  layer was verified by Convergent Beam Electron Diffraction (CBED) studies (not shown), which confirmed N-polarity in the  $\text{Al}_x\text{Ga}_{1-x}\text{N}$  film. However, there appear to be isolated regions of mixed polarity in the GaN buffer layer, as shown by two atomic resolution images of different GaN regions, which suggest that both N- and Ga-polar regions occur. This may be due to isolated N-polar regions forming by growth on

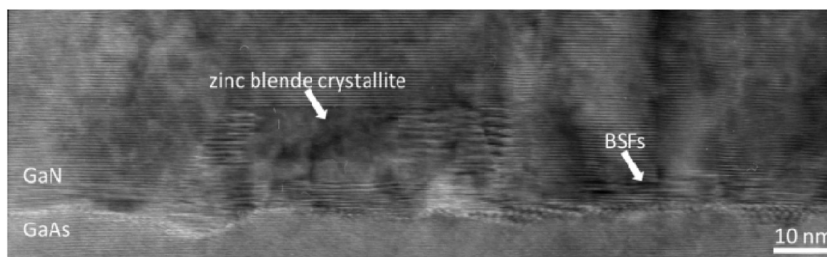


Fig. 26.. A high resolution TEM image of the GaN/GaAs interface [69].

meltback-etched regions of the GaAs substrate. However, no inversion domain boundaries were observed in the buffer region, so it is not known whether these mixed polarity regions occur in high densities. The high density of extended defects in the GaN buffer layer resulted in scattering effects in CBED patterns, preventing conclusive CBED information about GaN buffer film polarity to be measured.

Previous studies demonstrated that to achieve the highest growth rate of  $\sim 7.6 \mu\text{m/h}$  one needs to use a very high nitrogen flow of  $\sim 25 \text{ sccm}$  [66,67]. In order to grow thick  $\text{Al}_x\text{Ga}_{1-x}\text{N}$  layers in our conventional MBE system with the standard pumping configuration we used relatively low nitrogen flow rates of  $\sim 6 \text{ sccm}$ . That enabled us to grow thick  $\text{Al}_x\text{Ga}_{1-x}\text{N}$  layers with our CT-8 cryopump pumping system without frequent regeneration of the cryopump. The beam equivalent nitrogen pressure in the chamber during growth did not exceed  $2 \times 10^{-4} \text{ Torr}$ .

First we studied the growth rate of GaN as a function of Ga flux to determine the transition from N-rich to Ga-rich growth mode. For this purpose we grew GaN films at nitrogen flow rates of 6 sccm with an RF power of 500 W. Films grown under N-rich conditions were free from Ga droplets, which were clearly visible under Ga-rich conditions. Fig. 28 shows that the maximum growth rate achieved in this study was  $\sim 3 \mu\text{m/h}$ , which is consistent with previous studies using the Riber source [66]. From the above data we determined the Ga flux corresponding to the transition from N-rich to Ga-rich growth. Using that information we have grown a set of  $\text{Al}_x\text{Ga}_{1-x}\text{N}$  layers under slightly group III-rich conditions with an AlN content of about 20 mol%.

Fig. 29 demonstrates that the  $\text{Al}_x\text{Ga}_{1-x}\text{N}$  layer thickness increases linearly with growth time. We have observed a growth rate of  $\sim 2.2 \mu\text{m/h}$ , which is lower than we can see on sapphire wafers under similar conditions. This is probably result of different growth surface temperature or different Ga(Al) re-evaporation on sapphire and GaAs substrates, but this question is still under investigation.

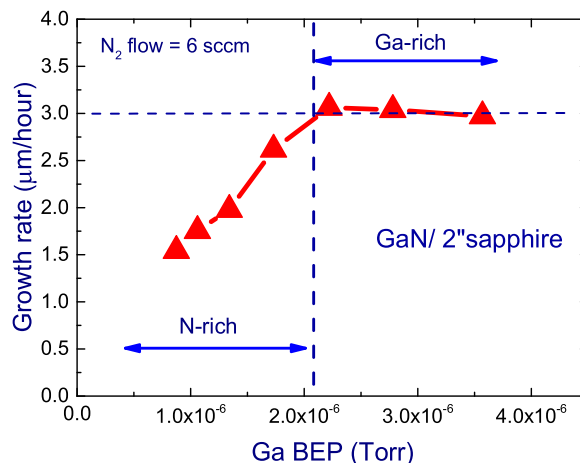


Fig. 28.. Growth rate dependence for GaN layers on 2-inch sapphire on the Ga flux for the Riber plasma source.

In  $2\theta$ - $\omega$  XRD plots we observed a shift of the  $\text{Al}_x\text{Ga}_{1-x}\text{N}$  peak to higher angle in comparison with a pure GaN layers, indicating a small decrease in lattice parameter in agreement with the literature. As shown in Fig. 30 for a  $100 \mu\text{m}$  thick wurtzite  $\text{Al}_x\text{Ga}_{1-x}\text{N}$  layers we observe a single 0002 reflection at  $\sim 35^\circ$ , which using Vegards law is consistent with the AlN mole fraction  $x \sim 0.2$ . This estimate of the AlN mole fraction was also confirmed by both energy dispersive X-Ray analysis (EDX) and SIMS studies. XRD measurements show that the zinc-blende content was below the detection limit (0.1%).

Figs. 31 and 32 shows the full-width-at-half -maximum (FWHM) of the 0002 peak at  $\sim 35^\circ$  from XRD  $\omega$ -plots for several wurtzite  $\text{Al}_x\text{Ga}_{1-x}\text{N}$  layers grown on 3-inch GaAs as a function of growth time. The  $\text{Al}_x\text{Ga}_{1-x}\text{N}$

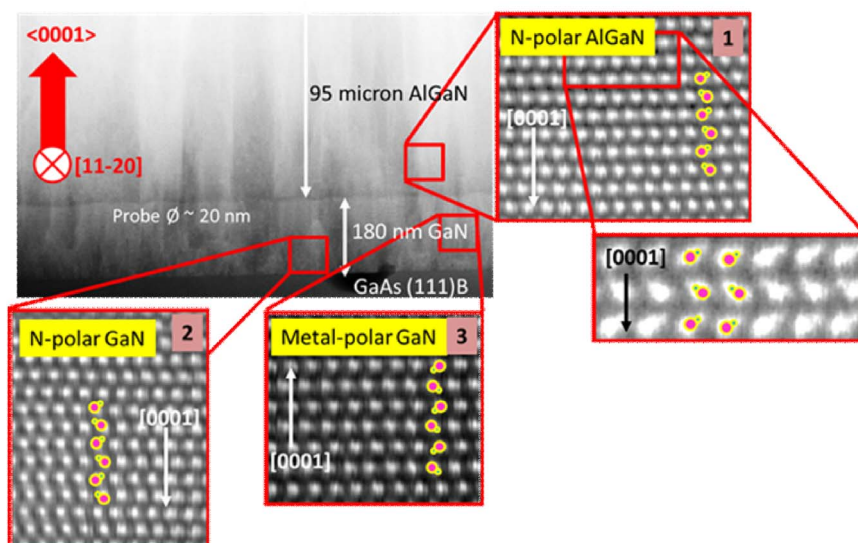


Fig. 27.. HR-STEM image of the AlGaN/GaN/GaAs (111) B substrate interface [71].

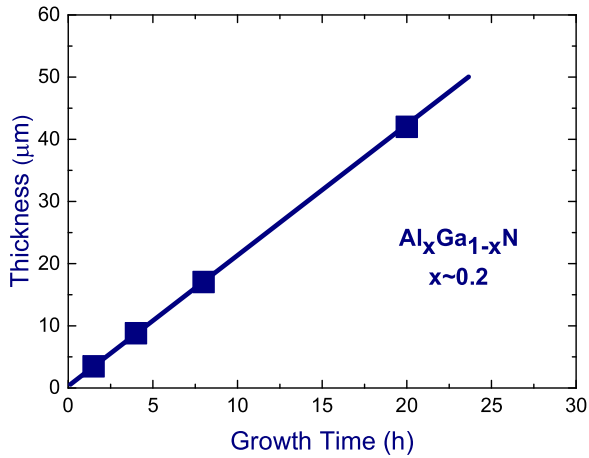


Fig. 29.. Thickness dependence on the growth time for  $\text{Al}_x\text{Ga}_{1-x}\text{N}$  layers ( $x \sim 0.2$ ) on 2-inch sapphire (6 sccm  $\text{N}_2$  flow at 500 W).

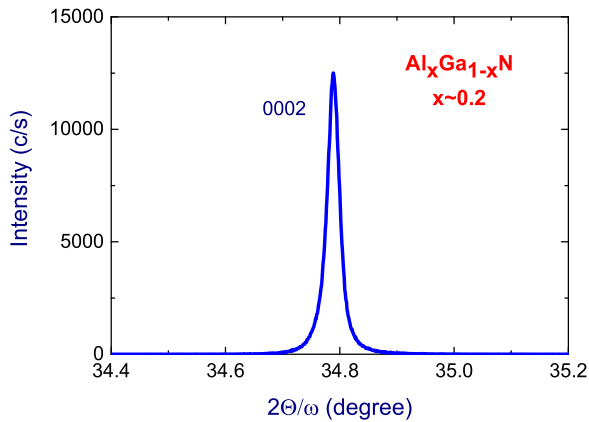


Fig. 30.. XRD scan of  $2\theta-\omega$  of the 0002 peak for a wurtzite  $\text{Al}_x\text{Ga}_{1-x}\text{N}$  layer.

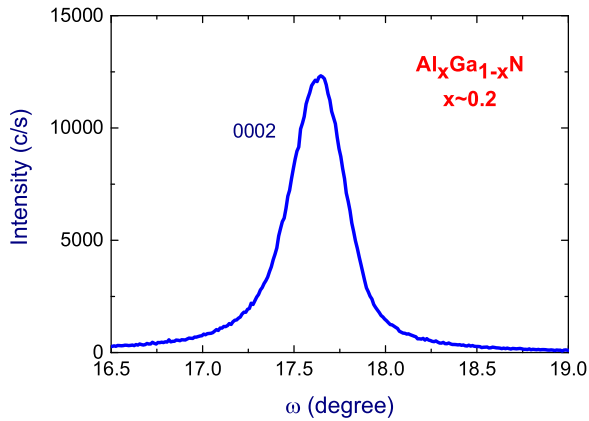


Fig. 31.. XRD  $\omega$ -plot of the 0002 peak for a wurtzite  $\text{Al}_x\text{Ga}_{1-x}\text{N}$  layer ( $x \sim 0.2$ , thickness  $\sim 100 \mu\text{m}$ ).

$x\text{N}$  layers were grown at a growth rate of  $\sim 2.2 \mu\text{m/h}$  and with an AlN content of  $x \sim 0.2$ . The growth time was up to 50 h and the thickness of the layers was up to  $\sim 100 \mu\text{m}$ . In all of our earlier experiments with the growth of free-standing zinc-blende  $\text{Al}_x\text{Ga}_{1-x}\text{N}$  layers, we observed degradation of the crystal quality of the layers with increasing thickness due to a gradual build-up of the concentration of wurtzite inclusions in the zinc-blende matrix. In the current research, the structural quality of the wurtzite  $\text{Al}_x\text{Ga}_{1-x}\text{N}$  layer improves rapidly with increasing layer thickness during the first few hours of growth. This is due to cubic inclusions close to the GaN/GaAs interface reverting to wurtzite. There is also a steady reduction in the density of stacking faults in the film,

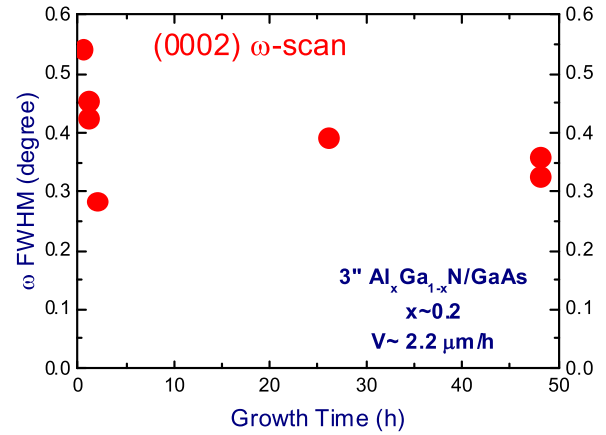


Fig. 32.. Dependence of  $\omega$  XRD 0002 peak FWHM for a wurtzite  $\text{Al}_x\text{Ga}_{1-x}\text{N}$  layers on the growth time.

which are readily generated by growth on mixed phase material close to the GaN/GaAs interface. However, we are still investigating the mechanisms behind that. The structural quality of  $\text{Al}_x\text{Ga}_{1-x}\text{N}$  then slightly degrades during further MBE growth. This may arise because we are probably shifting from the optimum growth temperature and Ga/N flux ratio after the first ten hours of growth, due to depletion of Ga in the Ga SUMO-cell during the long growths with high fluxes of BEP  $\sim 2 \times 10^{-6}$  Torr.

SIMS studies of wurtzite  $\text{Al}_x\text{Ga}_{1-x}\text{N}$  show that the Al, Ga and N profiles are uniform with depth within experimental error. There was no significant As detected in the SIMS profiles.

Photoluminescence (PL) studies show an increase in room temperature peak energy with increasing AlN content again as previously observed in the literature. Fig. 33 shows that we observe strong room temperature luminescence from the surface of a  $100 \mu\text{m}$  thick layer, suggesting the sample is of good optical quality. The energy of the PL peak is about 100 meV lower than expected for  $\text{Al}_{0.2}\text{Ga}_{0.8}\text{N}$ , assuming zero bowing factor, which suggests the peak may be due to donor-acceptor pair recombination.

Free-standing  $\text{Al}_x\text{Ga}_{1-x}\text{N}$  wafers with thicknesses in the 30 to  $100 \mu\text{m}$  range may be used as substrates for further growth of  $\text{Al}_x\text{Ga}_{1-x}\text{N}$ -based structures and devices. The novel high efficiency RF plasma source allowed us to achieve such  $\text{Al}_x\text{Ga}_{1-x}\text{N}$  thicknesses on 3-inch diameter wafers in a single day's growth (Fig. 34), which makes our growth technique potentially commercially viable.

### 1.9. Boron impurities in MBE GaN and $\text{Al}_x\text{Ga}_{1-x}\text{N}$ layers

Many years ago it became clear that in PA-MBE using a nitrogen RF

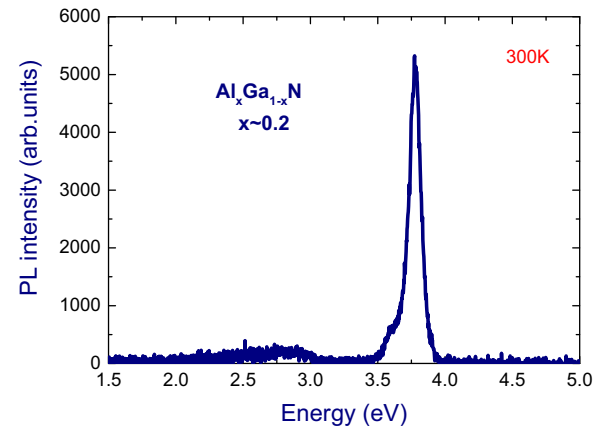


Fig. 33.. Room temperature PL of wurtzite  $\text{Al}_x\text{Ga}_{1-x}\text{N}$  layer ( $x \sim 0.2$ , thickness  $\sim 100 \mu\text{m}$ ).



Fig. 34.. Part of a 3-inch wurtzite  $\text{Al}_x\text{Ga}_{1-x}\text{N}$  wafer on glass  $x \sim 0.2$  and thickness  $\sim 57 \mu\text{m}$ .

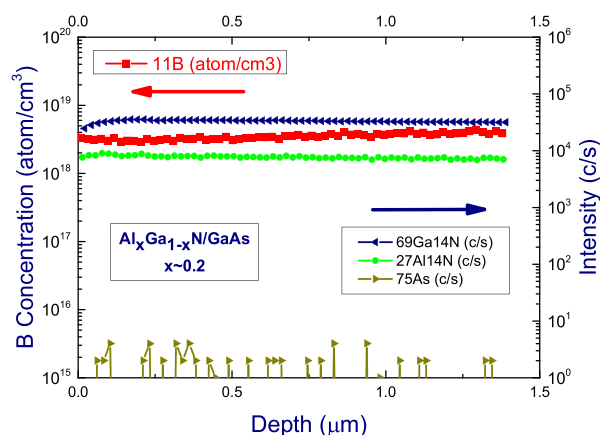


Fig. 35.. SIMS profiles for B, Ga, Al and As for a top surface of  $w\text{-Al}_x\text{Ga}_{1-x}\text{N}$  layer ( $x \sim 0.2$ ) with the thickness  $\sim 95 \mu\text{m}$  grown with the highly efficient Ribber RF plasma source.

plasma source there is unintentional doping of the layers with boron (B) due to decomposition of either the pyrolytic boron nitride (PBN) cavity or the PBN aperture plate of the RF plasma source or both [73]. It was established that the boron background concentration in unintentionally doped GaN depended strongly on the RF power for the plasma nitrogen source [74].

During the last few years, we have compared different RF nitrogen plasma sources for the growth of thick free-standing wurtzite  $\text{Al}_x\text{Ga}_{1-x}\text{N}$  films. We are using a highly efficient RF plasma source with high nitrogen flows and high RF powers. Our GaN growth rates reached  $3 \mu\text{m/h}$ , which is about one order of magnitude higher than in our earlier studies. Therefore, one can expect that the PBN cavity decomposition and unintentional B incorporation could become significantly more intense.

We have studied several  $\text{Al}_x\text{Ga}_{1-x}\text{N}$  layers grown by MBE with the HD-25 plasma source and we have observed similar boron incorporation levels similar  $\sim 7\text{--}8 \times 10^{17} \text{ cm}^{-3}$  [75]. For growth of the  $\text{Al}_x\text{Ga}_{1-x}\text{N}$  layers we have used group III-rich conditions and a growth rates of  $\sim 0.25 \mu\text{m/h}$ . The boron concentration was quantified by SIMS using reference samples of boron implanted standards.

Fig. 35 shows SIMS profiles for B for a  $w\text{-Al}_x\text{Ga}_{1-x}\text{N}$  layer ( $x \sim 0.2$ ) grown with the highly efficient Ribber RF plasma source. We have grown the  $\text{Al}_x\text{Ga}_{1-x}\text{N}$  layer on a 2-inch GaAs substrate for  $\sim 45$  hours under group III-rich conditions, with a growth rate  $\sim 2.25 \mu\text{m/h}$ . Using SIMS, it is not cost effective to try to sputter through the entire  $\sim 100 \mu\text{m}$  of the layer to see the  $\text{Al}_x\text{Ga}_{1-x}\text{N}/\text{GaAs}$  interface. Therefore, Fig. 35 presents SIMS data from the top  $\sim 1.5 \mu\text{m}$  of  $w\text{-Al}_x\text{Ga}_{1-x}\text{N}$  layer. The arsenic concentration is below or just on the level of sensitivity of SIMS

system. The boron concentration in  $\text{Al}_x\text{Ga}_{1-x}\text{N}$  layer is uniform through the layer and is  $\sim 3 \times 10^{18} \text{ cm}^{-3}$ . It is very important to highlight the fact that the boron concentration in the  $\text{Al}_x\text{Ga}_{1-x}\text{N}$  layers presented was practically identical and has not changed after 2 days of continuous MBE growth using the Ribber RF plasma source. We have studied several  $\text{Al}_x\text{Ga}_{1-x}\text{N}$  layers grown under similar MBE growth conditions with the Ribber plasma source on 2-inch and 3-inch GaAs substrates and we have observed similar levels of boron incorporation to that shown in Fig. 35.

The growth rate for  $\text{Al}_x\text{Ga}_{1-x}\text{N}$  layers achieved with the Ribber source is  $\sim 2.2 \mu\text{m/h}$ , which is  $\sim 10$  times faster than that for the layers grown with the HD-25 source of  $\sim 0.25 \mu\text{m/h}$ . However, the boron concentration is only 4 times higher and increased from  $\sim 7\text{--}8 \times 10^{17} \text{ cm}^{-3}$  to  $\sim 3 \times 10^{18} \text{ cm}^{-3}$ . Therefore, boron doping concentration in the layer is increasing for the GaN layers grown with the highly efficient source, but not as fast as the increase in growth rate. To understand this let's consider the growth parameters, which will influence the boron incorporation. The boron concentration in the layer will be equal to the total number of boron atoms in the GaN layer divided by the total volume of the GaN layer. Therefore, boron concentration is proportional to the boron flux divided by the growth rate [75]. This means that if, for example, the growth rate increases by a factor 10 and the boron flux also increases by a factor 10, the resulting boron concentration in the GaN will not change at all. Therefore, we can see that we have strong increase in the boron flux coming from the highly efficient RF plasma source. However, this resulted in a relatively small increase in the boron concentration, because the growth rate is also higher. Therefore, the level of unintentional boron doping in GaN layers grown with a highly efficient plasma sources is only a few times higher than the boron concentration in layers grown with a standard RF plasma sources. Therefore, we can conclude that boron incorporation with this highly efficient RF plasma source is approximately  $3 \times 10^{18} \text{ cm}^{-3}$  for the  $\text{Al}_x\text{Ga}_{1-x}\text{N}$  growth rates of  $2\text{--}3 \mu\text{m/h}$ .

## 2. Summary

In this review we have discussed the growth of free-standing zinc-blende (cubic) and wurtzite (hexagonal) GaN and  $\text{Al}_x\text{Ga}_{1-x}\text{N}$  layers by plasma assisted molecular beam epitaxy (PA-MBE). We have produced, for the first time, free-standing layers of zinc-blende GaN and  $\text{Al}_x\text{Ga}_{1-x}\text{N}$  up to  $100 \mu\text{m}$  in thickness and up to 3-inch in diameter. We have shown that our newly developed PA-MBE process for the growth of thick zinc-blende GaN layers can also be used to achieve free-standing wurtzite  $\text{Al}_x\text{Ga}_{1-x}\text{N}$  wafers. We have demonstrated controlled doping and Al composition control for free-standing  $\text{Al}_x\text{Ga}_{1-x}\text{N}$  layers. At a thickness of  $\sim 30 \mu\text{m}$ , free-standing GaN and AlGaN wafers can easily be handled without cracking. Therefore, free-standing GaN and  $\text{Al}_x\text{Ga}_{1-x}\text{N}$  wafers with thicknesses in the  $30\text{--}100 \mu\text{m}$  range may be used as substrates for further growth of GaN and  $\text{Al}_x\text{Ga}_{1-x}\text{N}$ -based structures and devices. Using the new high efficiency plasma sources it is possible to grow such free-standing cubic and hexagonal GaN and  $\text{Al}_x\text{Ga}_{1-x}\text{N}$  layers in a single day making PA-MBE a potentially viable commercial process.

## Acknowledgements

This work was undertaken with support from the Engineering and Physical Sciences Research Council UK (GR/S23582/01, EP/G046867/1, EP/K008323/1) and DTI UK grant SULFIA. We want to acknowledge Loughborough Surface Analysis Ltd for SIMS measurements and discussions of results.

## References

- [1] O. Ambacher, J. Majewski, C. Miskys, A. Link, M. Hermann, M. Eickhoff, M. Stutzmann, F. Bernardini, V. Fiorentini, V. Tilak, B. Schaff, L.F. Eastman, Pyroelectric properties of  $\text{Al}(\text{In})\text{GaN}/\text{GaN}$  hetero- and quantum well structures, *J. Phys.* 14 (2002) 3399–3434.

- [2] P. Waltereit, O. Brandt, M. Ramsteiner, R. Uecker, P. Reiche, K.H. Ploog, Growth of M-plane GaN(1-100) on  $\gamma$ -LiAlO<sub>2</sub>(100), *J. Cryst. Growth* 218 (2000) 143–147.
- [3] S. Tripathy, R.K. Soni, H. Asahi, K. Iwata, R. Kuroiwa, K. Asami, S. Gonda, Optical properties of GaN layers grown on C-, A-, R-, and M-plane sapphire substrates by gas source molecular beam epitaxy, *J. Appl. Phys.* 85 (1999) 8386–8399.
- [4] B.A. Haskell, F. Wu, S. Matsuda, M.D. Craven, P.T. Fini, S.P. DenBaars, J.S. Speck, S. Nakamura, Structural and morphological characteristics of planar (11-20) a-plane gallium nitride grown by hydride vapor phase epitaxy, *Appl. Phys. Lett.* 83 (2003) 1554–1556.
- [5] M. Mizuta, S. Fujieda, Y. Matsumoto, T. Kawamura, Low temperature growth of GaN and AlN on GaAs utilizing metalorganics and hydrazine, *Jap. J. Appl. Phys.* 25 (1986) L945–L948.
- [6] M.J. Paisley, Z. Sitar, J.B. Posthill, R.F. Davis, Growth of cubic phase gallium nitride by modified molecular-beam epitaxy, *J. Vac. Sci. Technol. A* 7 (1989) 701–705.
- [7] S. Strite, H. Morkoc, GaN, AlN, and InN: a review, *J. Vac. Sci. Technol. B* 10 (1992) 1237–1266.
- [8] S. Strite, D. Chandrasekhar, D.J. Smith, J. Sariel, H. Chen, N. Teraguchi, H. Morkoc, Structural properties of InN films grown on GaAs substrates: observation of the zincblende polytype, *J. Cryst. Growth* 127 (1993) 204–208.
- [9] T. Lei, K.F. Ludwig, T.D. Moustakas, Heteroepitaxy, polymorphism, and faulting in GaN thin films on silicon and sapphire substrates, *J. Appl. Phys.* 74 (1993) 4430–4437.
- [10] R.G. Powell, N.E. Lee, Y.W. Kim, J.E. Greene, Heteroepitaxial wurtzite and zincblende structure GaN grown by reactive-ion molecular-beam epitaxy: growth kinetics, microstructure, and properties, *J. Appl. Phys.* 73 (1993) 189–204.
- [11] H. Liu, A.C. Frenkel, J.G. Kim, R.M. Park, Growth of zinc blende-GaN on  $\beta$ -SiC coated (001) Si by molecular beam epitaxy using a radio frequency plasma discharge, nitrogen free-radical source, *J. Appl. Phys.* 74 (1993) 6124–6127.
- [12] T.S. Cheng, L.C. Jenkins, S.E. Hooper, C.T. Foxon, J.W. Orton, D.E. Lacklison, Selective growth of zinc-blende, wurtzite, or a mixed phase of gallium nitride by molecular beam epitaxy, *Appl. Phys. Lett.* 66 (1995) 1509–1511.
- [13] O. Brandt, H. Yang, B. Jenichen, Y. Suzuki, L. Daweritz, K.H. Ploog, Surface reconstructions of zinc-blende GaN/GaAs(001) in plasma-assisted molecular-beam epitaxy, *Phys. Rev. B* 52 (1995) R2253–R2256.
- [14] D. Schikora, M. Hankeln, D.J. As, K. Lischka, T. Litz, A. Waag, T. Buhrow, F. Henneberger, Epitaxial growth and optical transitions of cubic GaN films, *Phys. Rev. B* 54 (1996) R8381–R8384.
- [15] L. Shunfeng, J. Schomann, D.J. As, K. Lischka, Room temperature green light emission from nonpolar cubic InGaN/GaN multi-quantum-wells, *Appl. Phys. Lett.* 90 (2007) 071903.
- [16] D.J. As, D. Schikora, A. Greiner, M. Lubbers, J. Mimkes, K. Lischka, p- and n-type cubic GaN epilayers on GaAs, *Phys. Rev. B* 54 (1996) R11118–R11121.
- [17] K.T. Delaney, P. Rinke, C.G. Van de Walle, Auger recombination rates in nitrides from first principles, *Appl. Phys. Lett.* 94 (2009) 191109.
- [18] H. Tsuchiya, K. Sunaba, T. Suemasu, F. Hasegawa, Growth of thick and pure cubic GaN on (001) GaAs by halide VPE, *J. Cryst. Growth* 198/199 (1999) 1056–1060.
- [19] T. Schupp, K. Lishka, D.J. As, MBE growth of atomically smooth non-polar cubic AlN, *J. Cryst. Growth* 312 (2010) 1500–1504.
- [20] M. Roppischer, R. Goldhahn, G. Rossbach, P. Schley, C. Cobet, N. Esser, T. Schupp, K. Lishka, D.J. As, Dielectric function of zinc-blende AlN from 1 to 20 eV: band gap and van Hove singularities, *J. Appl. Phys.* 106 (2009) 076104.
- [21] M.P. Thompson, G.W. Auner, A.R. Drews, Epitaxial growth of zinc-blende AlN on Si (100) substrates by plasma source molecular beam epitaxy, *J. Electron. Mater.* 28 (1999) L17–L19.
- [22] D. Gerthsen, B. Neubauer, Ch. Dieker, R. Lantier, A. Rizzi, H. Luth, Molecular beam epitaxy (MBE) growth and structural properties of GaN and AlN on 3C-SiC(001) substrates, *J. Cryst. Growth* 200 (1999) 353–361.
- [23] A. Nakadaira, H. Tanaka, Metalorganic vapor-phase epitaxy of cubic Al<sub>x</sub>Ga<sub>1-x</sub>N alloy on a GaAs (100) substrate, *Appl. Phys. Lett.* 70 (1997) 2720–2722.
- [24] V. Cimalla, V. Lebedev, U. Kaiser, R. Goldhahn, Ch. Foerster, J. Pezoldt, O. Ambacher, Polytype control and properties of AlN on silicon, *Phys. Status Sol. C* 2 (2005) 2199–2203.
- [25] T. Koizumi, H. Okumura, K. Balakrishnan, H. Harima, T. Inoue, Y. Ishida, T. Nagatomo, S. Nakashima, S. Yoshida, Growth and characterization of cubic AlGaIn and AlN epilayers by RF-plasma assisted MBE, *J. Cryst. Growth* 201/202 (1999) 341–345.
- [26] J.H. Edgar, S. Strite, I. Akasaki, H. Amano, C. Wetzel (Eds.), Gallium Nitride and Related Semiconductors, INSPEC, Stevenage, 1999 ISBN 0 85296 953 8.
- [27] M. Shatalov, W. Sun, A. Lunev, X. Hu, A. Dobrinsky, Y. Bilenko, J. Yang, M. Shur, R. Gaska, C. Moe, G. Garrett, M. Wraback, AlGaIn deep-ultraviolet light-emitting diodes with external quantum efficiency above 10%, *Appl. Phys. Express* 5 (2012) 082101.
- [28] H. Hirayama, N. Noguchi, T. Yatabe, N. Kamata, 227 nm AlGaIn light-emitting diode with 0.15 mW output power realized using a thin quantum well and AlN buffer with reduced threading dislocation density, *Appl. Phys. Express* 1 (2008) 051101.
- [29] Z. Ren, Q. Sun, S.-Y. Kwon, J. Hana, K. Davitt, Y.K. Song, A.V. Nurmikko, H.-K. Cho, W. Liu, J.A. Smart, L.J. Schowalter, Heteroepitaxy of AlGaIn on bulk AlN substrates for deep ultraviolet light emitting diodes, *Appl. Phys. Lett.* 91 (2007) 051116.
- [30] Z. Bryan, I. Bryan, S. Mita, J. Tweedie, Z. Sitar, R. Collazo, Strain dependence on polarization properties of AlGaIn and AlGaIn-based ultraviolet lasers grown on AlN substrates, *Appl. Phys. Lett.* 106 (2015) 232101.
- [31] A. Belousov, S. Katrych, J. Jun, J. Zhang, D. Gunther, R. Sobolewski, J. Karpinski, B. Batlogg, Bulk single-crystal growth of ternary Al<sub>x</sub>Ga<sub>1-x</sub>N from solution in gallium under high pressure, *J. Cryst. Growth* 311 (2009) 3971–3974.
- [32] Y.V. Melnik, V.A. Soukhoveev, K.V. Tsvetkov, V.A. Dmitriev, First AlGaIn free-standing wafers, *MRS Symp. Proc.* 764 (2003) 363–368.
- [33] S.V. Novikov, N.M. Stanton, R.P. Campion, R.D. Morris, H.L. Geen, C.T. Foxon, A.J. Kent, Growth and characterization of free-standing zinc-blende (cubic) GaN layers and substrates, *Semicond. Sci. Technol.* 23 (2008) 015018.
- [34] C.T. Foxon, S.V. Novikov, N.M. Stanton, R.P. Campion, A.J. Kent, Free-standing zinc-blende (cubic) GaN substrates grown by a molecular beam epitaxy process, *Phys. Stat. Sol. B* 245 (2008) 890–892.
- [35] S.V. Novikov, N.M. Stanton, R.P. Campion, C.T. Foxon, A.J. Kent, Free-standing zinc-blende (cubic) GaN layers and substrates, *J. Cryst. Growth* 310 (2008) 3964–3967.
- [36] I. Grzegory, S. Krukowski, M. Leszczynski, P. Perlin, T. Suski, S. Porowski, The application of high pressure in physics and technology of III-V nitrides, *Acta Phys. Pol. A* 100 (2001) 57–109.
- [37] S.V. Novikov, N. Zainal, A.V. Akimov, C.R. Staddon, A.J. Kent, C.T. Foxon, Molecular beam epitaxy as a method for the growth of freestanding zinc-blende (cubic) GaN layers and substrates, *J. Vac. Sci. Technol. B* 28 (2010) C3B1–C3B6.
- [38] S.V. Novikov, C.T. Foxon, A.J. Kent, Growth and characterization of free-standing zinc-blende GaN layers and substrates, *Phys. Stat. Sol. A* 207 (2010) 1277–1282.
- [39] S.V. Novikov, C.T. Foxon, A.J. Kent, Zinc-blende (cubic) GaN bulk crystals grown by molecular beam epitaxy, *Phys. Stat. Sol. C* 8 (2011) 1439–1444.
- [40] B. Heying, R. Averbek, L.F. Chen, E. Haus, H. Riechert, J.S. Speck, Control of GaN surface morphologies using plasma-assisted molecular beam epitaxy, *J. Appl. Phys.* 88 (2000) 1855–1860.
- [41] H. Yaguchi, J. Wu, H. Akiyama, M. Baba, K. Onabe, Y. Shiraki, Time-resolved photoluminescence of cubic GaN grown by metalorganic vapor phase epitaxy, *Phys. Stat. Sol. B* 216 (1999) 237–240.
- [42] A. Philippe, C. Bru-Chevallier, M. Vernay, G. Guillot, J. Hubner, B. Daudin, G. Feuillet, Optical properties of cubic GaN grown on SiC/Si substrates, *Mat. Sci. Eng. B* 59 (1999) 168–172.
- [43] K. Lischka, Heteroepitaxy of cubic GaN, *Brazilian J. Phys.* 27 (1997) 80–87.
- [44] N. Zainal, S.V. Novikov, A.V. Akimov, C.R. Staddon, C.T. Foxon, A.J. Kent, Hexagonal (wurtzite) GaN inclusions as a defect in cubic (zinc-blende) GaN, *Physica B* 407 (2012) 2964–2966.
- [45] S.V. Novikov, N. Zainal, C.T. Foxon, A.J. Kent, F. Luckert, P.R. Edwards, R.W. Martin, Study of unintentional arsenic incorporation into free-standing zinc-blende GaN and AlGaIn layers grown by molecular beam epitaxy on GaAs substrates, *Phys. Stat. Sol. C* 7 (2010) 2033–2035.
- [46] S.V. Novikov, R.E.L. Powell, C.R. Staddon, A.J. Kent, C.T. Foxon, Doping of free-standing zinc-blende GaN layers grown by molecular beam epitaxy, *J. Cryst. Growth* 403 (2014) 43–47.
- [47] R.E.L. Powell, S.V. Novikov, C.T. Foxon, A.V. Akimov, A.J. Kent, Photoluminescence of magnesium and silicon doped cubic GaN, *Phys. Stat. Sol. C* 11 (2014) 385–388.
- [48] D.J. As, K. Lischka, Heteroepitaxy of doped and undoped cubic group III-nitrides, *Phys. Stat. Sol. A* 176 (1999) 475–485.
- [49] S.V. Novikov, N. Zainal, A.V. Akimov, C.R. Staddon, C.T. Foxon, A.J. Kent, D.P. Nicholls, S.E. Hooper, Zinc-blende (cubic) GaN/InGaIn optoelectronic device structures on (001) free-standing cubic GaN substrates both grown by molecular beam epitaxy, *Proc.: The 8th International Conference on Nitride Semiconductors*, Jeju, Korea, October 18–23, 2009, pp. 494–495.
- [50] P.L. Kuhns, A. Kleinhammes, T. Schmiel, W.G. Moulton, P. Chabrier, S. Sloan, E. Hughes, C.R. Bowers, Magnetic-field dependence of the optical Overhauser effect in GaAs, *Phys. Rev. B* 55 (1997) 7824–7830.
- [51] C.A. Michal, R. Tycko, Stray-field NMR imaging and wavelength dependence of optically pumped nuclear spin polarization in InP, *Phys. Rev. B* 60 (1999) 8672–8679.
- [52] R. Tycko, Optical pumping in indium phosphide: <sup>31</sup>P NMR measurements and potential for signal enhancement in biological solid state NMR, *Solid State NMR* 11 (1998) 1–9.
- [53] S.V. Novikov, R.D. Morris, A.J. Kent, H.L. Geen, C.T. Foxon, MBE growth of GaN using <sup>15</sup>N isotope for nuclear magnetic resonance applications, *J. Cryst. Growth* 301-302 (2007) 417–419.
- [54] S.V. Novikov, C.R. Staddon, C.T. Foxon, F. Luckert, P.R. Edwards, R.W. Martin, A.J. Kent, Molecular beam epitaxy as a method for the growth of free-standing bulk zinc-blende GaN and AlGaIn crystals, *J. Cryst. Growth* 323 (2011) 80–83.
- [55] T. Schupp, K. Lishka, D.J. As, MBE growth of atomically smooth non-polar cubic AlN, *J. Cryst. Growth* 312 (2010) 1500–1504.
- [56] R.E.L. Powell, S.V. Novikov, F. Luckert, P.R. Edwards, A.V. Akimov, C.T. Foxon, R.W. Martin, A.J. Kent, Carrier localization and related photoluminescence in cubic AlGaIn epilayers, *J. Appl. Phys.* 110 (2011) 063517.
- [57] T. Suzuki, H. Yaguchi, H. Okumura, Y. Ishida, S. Yoshida, Optical constants of cubic GaN, AlN, and AlGaIn alloys, *Jpn. J. Appl. Phys.* 39 (2000) L497–L499.
- [58] M. Marques, L.K. Teles, L.M.R. Scolafo, J.R. Leite, J. Furthmuller, F. Bechstedt, Lattice parameter and energy band gap of cubic Al<sub>x</sub>Ga<sub>1-x</sub>In<sub>1-x-y</sub>N quaternary alloys, *Appl. Phys. Lett.* 83 (2003) 890–892.
- [59] C.J. Collins, A.V. Sampath, G.A. Garrett, W.L. Sarney, H. Shen, M. Wraback, A.Yu. Nikiforov, G.S. Cargill, V. Dierolf, Enhanced room-temperature luminescence efficiency through carrier localization in Al<sub>x</sub>Ga<sub>1-x</sub>N alloys, *Appl. Phys. Lett.* 86 (2005) 031916.
- [60] A. Klochikhin, A. Reznitsky, S. Permogorov, T. Breitkopf, M. Grun, M. Hetterich, C. Klingshirn, V. Lyssenko, W. Langbein, J.M. Hvam, Luminescence spectra and kinetics of disordered solid solutions, *Phys. Rev. B* 59 (1999) 12947–12972.
- [61] L. He, M.A. Reshchikov, F. Yun, D. Huang, T. King, H. Morkoc, Properties of Al<sub>x</sub>Ga<sub>1-x</sub>N layers grown by plasma-assisted molecular-beam epitaxy under Ga-rich conditions, *Appl. Phys. Lett.* 81 (2002) 2178–2180.
- [62] E. Iliopoulos, K.F. Ludwig, T.D. Moustakas, S.N.G. Chu, Chemical ordering in AlGaIn alloys grown by molecular beam epitaxy, *Appl. Phys. Lett.* 78 (2001) 463–465.

- [63] S.V. Novikov, C.R. Staddon, R.E.L. Powell, A.V. Akimov, F. Luckert, P.R. Edwards, R.W. Martin, A.J. Kent, C.T. Foxon, Wurtzite  $\text{Al}_x\text{Ga}_{1-x}\text{N}$  bulk crystals grown by molecular beam epitaxy, *J. Cryst. Growth* 322 (2011) 23–26.
- [64] S.V. Novikov, C.R. Staddon, F. Luckert, P.R. Edwards, R.W. Martin, A.J. Kent, C.T. Foxon, Zinc-blende and wurtzite  $\text{Al}_x\text{Ga}_{1-x}\text{N}$  bulk crystals grown by molecular beam epitaxy, *J. Cryst. Growth* 350 (2012) 80–84.
- [65] S.V. Novikov, C.R. Staddon, R.W. Martin, A.J. Kent, C.T. Foxon, Molecular beam epitaxy of free-standing wurtzite  $\text{Al}_x\text{Ga}_{1-x}\text{N}$  layers, *J. Cryst. Growth* 425 (2015) 125–128.
- [66] B.M. McSkimming, F. Wua, T. Huault, C. Chaix, J.S. Speck, Plasma assisted molecular beam epitaxy of GaN with growth rates  $> 2.6 \mu\text{m}/\text{h}$ , *J. Cryst. Growth* 386 (2014) 168–174.
- [67] B.M. McSkimming, C. Chaix, J.S. Speck, High active nitrogen flux growth of GaN by plasma assisted molecular beam epitaxy, *J. Vac. Sci. Technol. A* 33 (2015) 05E128.
- [68] B.P. Gunning, E.A. Clinton, J.J. Merola, W.A. Doolittle, R.C. Bresnahan, Control of ion content and nitrogen species using a mixed chemistry plasma for GaN grown at extremely high growth rates  $> 9 \mu\text{m}/\text{h}$  by plasma-assisted molecular beam epitaxy, *J. Appl. Phys.* 118 (2015) 155302.
- [69] S.V. Novikov, C.R. Staddon, J. Whale, A.J. Kent, C.T. Foxon, Growth of free-standing wurtzite AlGa<sub>N</sub> by MBE using a highly efficient RF plasma source, *J. Vac. Sci. Technol. B* 34 (2016) 02L102.
- [70] S.V. Novikov, C.R. Staddon, S.-L. Sahonta, R.A. Oliver, C.J. Humphreys, C.T. Foxon, Molecular beam epitaxy of free-standing bulk wurtzite  $\text{Al}_x\text{Ga}_{1-x}\text{N}$  layers using a highly efficient RF plasma source, *Phys. Stat. Sol. C* 13 (2016) 217–220.
- [71] S.V. Novikov, C.R. Staddon, S.-L. Sahonta, R.A. Oliver, C.J. Humphreys, C.T. Foxon, Growth of free-standing bulk wurtzite  $\text{Al}_x\text{Ga}_{1-x}\text{N}$  layers by molecular beam epitaxy using a highly efficient RF plasma source, *J. Cryst. Growth* 456 (2016) 151–154.
- [72] O. Takahashi, T. Nakayama, R. Souda, F. Hasegawa, V/III Ratio Dependence of Polarity of GaN Grown on GaAs (111)A-Ga and (111)B-As Surfaces by MOMBE, *Phys. Stat. Sol. B* 228 (2001) 529–532.
- [73] R.M. Moldovan, L.S. Hirsch, A.J. Ptak, C.D. Stinespring, T.H. Myers, N.C. Giles, Nitrogen doping of ZnSe and CdTe epilayers: a comparison of two rf sources, *J. Electron. Mater.* 27 (1998) 756–762.
- [74] H. Kim, F.J. Falth, T.G. Andersson, Unintentional incorporation of B, As, and O impurities in GaN grown by molecular beam epitaxy, *J. Electron. Mater.* 30 (2001) 1343–1347.
- [75] S.V. Novikov, C.T. Foxon, Unintentional boron incorporation in AlGa<sub>N</sub> layers grown by plasma-assisted MBE using highly efficient nitrogen RF plasma-sources, *J. Cryst. Growth* (2017) accepted.